Title: Novel Pan-RAS Inhibitor ADT-007 Induces Tumor Regression in Mouse Models of GI Cancer

Authors: [1]*Jeremy B. Foote,* [2]*Tyler E. Mattox,* [3,10]*Adam B. Keeton,* [3]*Forrest Smith,* [3]*Kristly L. Berry,* [2]*Antonio B. Ward,* [3]*Karina J. Yoon,* [4]*Sujith Sarvesh,* [4]*Ganji P. Nagaraju,* [5]*Yulia Maxuitenko,* [5,10]*Xi Chen,* [5]*Jacob Valiyaveettil,* [4]*Julienne L. Carstens,* [6]*Jennifer Yang,* [7]*Donald J. Buchsbaum,* [8]*Gang Zhou,* [9]*Elmar Nurmmedov,* [9]*Ivan Babic,* [10]*Vadim Gaponenko,* [10]*Hazem Abdelkarim,* [11]*Michael R. Boyd,* [4]*Bassel F. El-Rayes,* [5,11]*Gary A. Piazza*

Affiliations: [1]Department of Microbiology, University of Alabama at Birmingham, Birmingham AL; [2]University of South Alabama, Mobile, AL; [3]Department of Pharmacology and Toxicology, University of Alabama at Birmingham, Birmingham AL;[4]Department of Hematology and Oncology, University of Alabama at Birmingham, Birmingham, AL; [5]Department of Drug Discovery and Development, Harrison College of Pharmacy, Auburn University, Auburn, AL; [6]University of Connecticut, Mansfield, CT, [7]Department of Obstetrics and Gynecology, University of Alabama at Birmingham, Birmingham, AL; [8]Georgia Cancer Center, University of Augusta, Augusta, GA: [9]*Nerd Bio LLC, San Diego;* [10]*CA Department of Biochemistry and Molecular Genetics, University of Illinois, Chicago, IL;* [11]*ADT Pharmaceuticals LLC Orange Beach, AL*.

Running Title: *A Novel Pan-RAS Inhibitor for KRAS Mutated GI Cancers*

Key Words: KRAS, Pan-RAS inhibitor, Pancreatic Ductal Adenocarcinoma, Colorectal Adenocarcinoma, T cells

Funding Sources: NIH/NCI R01CA254197 and R01CA238514

Corresponding Author: Gary A. Piazza, *W.W. Walker Endowed Professor, Department Head, Drug Discovery and Development, Director, Cancer Research Center,* Harrison College of

Pharmacy, Auburn University, Walker Building, 362 W. Thach Ave, Room 3306F, Auburn, AL.

Phone: 334-844-7409, gap0034@auburn.edu

ABSTRACT

Here we describe a novel class of pan-RAS inhibitor with highly potent and selective anticancer activity by killing cancer cells harboring mutations in RAS or with constitutively activated RAS resulting from mutations in upstream signaling components. A lead compound from this chemical family, ADT-007, binds RAS when in a nucleotide free transitional state to block loading of GTP, thereby interfering with RAS activation and disruption of binding to effectors such as RAF and PI3K to suppress MAPK and AKT signaling. ADT-007 potently inhibits the growth of cultured human and murine cancer cell lines with single-digit nM IC_{50} values irrespective of specific RAS isozyme or mutational codon. ADT-007 also inhibits tumor growth *in vivo* through inhibition of RAS-MAPK signaling in syngeneic, immune competent and xenogeneic, immune deficient mouse models of colon and pancreatic cancer. In RAG 1 $^{-/-}$ mice the activity of ADT-007 is partially inhibited indicating a role for the adaptive immune system in ADT-007-mediated tumor growth inhibition. *Ex vivo* analyses of tumor infiltrating leukocytes, reveals that ADT-007 enhances T cell functions in the pancreatic and colorectal tumor immune microenvironment.

SIGNIFICANCE: ADT-007 represents a 1st-in-class pan-RAS inhibitor with broad anticancer activity across all RAS driven cancers and unique chemical selectivity to allow normal cells to be spared from pan-RAS inhibition. ADT-007 also has the potential to modulate the adaptive immune response in colorectal cancer (CRC) and pancreatic ductal adenocarcinoma (PDA). These data support future clinical trials of an orally bioavailable prodrug of ADT-007 as a monotherapy for the treatment of patients with CRC or PDAC regardless of the underlying mutation or in combination with immunotherapy.

BACKGROUND: CRC and PDAC are the 3rd (3rd most common cancer) and 4th (~9th most common cancer) leading causes of cancer-related deaths in the US in 2023 (1). It is projected that CRC and PDAC will cause 52,580 and 49,830 deaths in the US in 2023, respectively (1).

The 5-year survival rates for CRC and PDAC are 65% and 12%, respectively (1) Over 50% of CRC and 90% of pancreatic tumors have mutations in RAS genes that are associated with worse prognosis, making development of more effective treatments a priority (2).

Multiple mutations in the *KRAS* gene encode for constitutively activated KRAS proteins that act as oncogenic drivers in over 90% of patients with PDAC and about 25% of all human cancers. For many cancers, RAS mutations initiate tumor progression that in cooperation with the acquisition of mutations in other oncogenes or inactivating mutations in tumor suppressor genes such as p53 (3), SMAD4 (4), or p16 (5), promote the progression from precancerous lesions to malignant disease. Signaling through oncogenic KRAS is critical for tumor metabolism (6), chemo-resistance (7), and metastasis (8) (9). Oncogenic $KRAS^{G12D}$ signaling promotes immunosuppression within the tumor microenvironment (TME) through a broad array of mechanisms. Suppressive pathways include increased production of acute inflammatory cytokines (IL-6, IL-8) (10) (11) (12), priming of immunosuppressive T-regs (13), and MDSCs (14) (15), downregulation of MHCI (16), increased expression of programmed cell death ligand 1 (PD-L1) (17) (18), and suppression of intratumoral interferon (IFN) signaling (19). Cumulatively, oncogenic KRAS-mediated reprograming of the TME results in weakened recognition and reduced cytotoxic T and NK cell functions that support tumor progression.

Recent development of drugs directed against tumors harboring KRAS mutations at the G12C and G12D codons have set the stage for selective targeting of KRAS driven cancers (20). Clinical trials evaluating sotorasib and adagrasib selective for the $KRAS^{G12C}$ mutation reveal promising anti-tumor activity in previously treated cancers (21). Preclinical data indicate critical roles for both G12C KRAS and newly developed G12D KRAS inhibitors in rewiring the immunosuppressive machinery that limits T cell recognition and cytotoxic activity (22) (23) (24) (25). Despite their promise in preclinical animal models and recent progress in patients, the response of different tumor types to KRAS G12C targeted drugs has been variable with best

results seen in non-small cell lung cancer (NSCLC) followed by CRC (21). A critical issue seen in a high percentage of patients treated with G12C inhibitors is adaptive resistance (26) (27) (28) (29) mechanisms that limits the efficacy of mutation specific KRAS inhibitors in patients with CRC and likely other GI cancers. These resistance pathways often involve polyclonal mutations involving wild-type (WT) RAS isozymes (K, H, N) or other pathway components (28) (29) making the development of pan-RAS inhibitors an attractive therapeutic option to dampen the RAS-related adaptive resistance circuitry. Pan RAS inhibitors provide an opportunity to treat patients with RAS mutated tumors in a generalized fashion for a broad range of malignancies including PDAC and CRC where the majority of patients have other mutations in the KRAS isozyme (2) (30).

Here we report on development of a novel pan-RAS inhibitor (ADT-007) derived from a chemical library based on indene modifications of the nonsteroidal anti-inflammatory drug (NSAID), sulindac, has been reported to inhibit cancer cell growth, although the mechanism of action is poorly understood (31, 32). The anti-cancer activities of sulindac and certain derivatives that share its indene scaffold is attributed to several cellular targets (in addition to cyclooxygenases 1 and 2), including cGMP PDE inhibition, IKK-β, PPAR-δ, RXR-α, SERCA, and NAG-1(33). Others have identified potential alternative cellular targets of indene derivatives, including tubulin (34), but of particular relevance to the present manuscript, sulindac and analogs were reported to directly inhibit and bind RAS (35, 36). Consistent with this, sulindac sulfide inhibited RAS-mediated transformation of fibroblasts (37) and the non-COX-inhibitory sulindac metabolite Exisulind selectively inhibited the development of HRAS mutant breast tumors (38). Additional analogs have been described which inhibit growth of RAS-driven cell lines , and directly bind RAS (39).

In this study, we examine the anticancer activity and mechanism of action of ADT-007, a novel pan-RAS inhibitor using human and mouse cancer cell lines. We also study its anticancer

activity and immune modulatory potential using preclinical mouse models of $KRAS^{G12D/V/C}$ driven CRC and PDAC.

RESULTS:

Potency and selectivity of ADT-007 to inhibit the growth of cancer cells with mutated or hyper-activated RAS

A focused library of indenes was synthesized and screened for differential growth inhibitory activity in full dose-response (9 concentrations 1-10,000 nM, 4 replicates each) using mutant *KRAS* (G13D) HCT116 CRC cells vs. WT *RAS*, mutant *BRAF* (V600E) HT29 colon cancer cells. Consistent with harboring a KRAS mutation, HCT116 CRC cells had high levels of activated RAS as measured by RAS-RBD pull-down assays, while WT KRAS HT29 CRC cells expressed essentially undetectable levels of activated RAS. However, both cell lines were responsive to MAPK inhibitors (data not shown), which supports the use of this pair to screen for a selective RAS inhibitor. A lead compound, ADT-007, emerged following extensive chemical optimization to optimize potency and selectivity by iterative screening. ADT-007 inhibits the growth of HCT116 CRC cells with an IC_{50} of 5 nM, while the IC_{50} for HT29 CRC cells was 93-fold higher (**Figure 1A**). Near complete killing was apparent in HCT116 cultures following 3-days of treatment. Continuous treatment with ADT-007 for up to 21 days did not affect the viability of WT KRAS HT29 cells (data not shown).

Long durations of treatment with ADT-007 (10 days) in colony formation assays resulted in even greater potency in which sub-nanomolar concentrations caused complete inhibition of colony formation of mutant KRAS HCT116 CRC cells without affecting colony formation of WT RAS HT29 CRC cells (**Figure 1B**). Other experiments showed selective apoptosis of mutant KRAS HCT116 CRC cells as measured by increased Annexin V levels (**Figure 1C**). Within the same concentration range for inducing apoptosis, ADT-007 also induced G2/M (mitotic) arrest in

HCT116 cells, while much higher concentrations (>100x higher) were needed to have a similar effect on cell cycle distribution in HT29 cells (**Figure 1D**). The induction of mitotic arrest in HCT116 CRC cells by ADT-007 treatment was confirmed by residual cells showing high levels of histone 3B expression, a marker of mitotic arrest (**Figure 1E**) (40). These findings show that ADT-007 potently and selectively inhibits the growth of mutant KRAS CRC cell lines by inducing mitotic arrest and apoptosis.

A panel of histologically diverse cancer cell lines with various mutations in *KRAS, HRAS*, and *NRAS*, as well as lines with mutations upstream of RAS leading to hyper-activation of WT RAS were evaluated along with cancer cell lines with WT RAS but with downstream RAF mutations, or cells from normal tissues (lung and colon) for *in vitro* sensitivity to ADT-007 growth inhibition assays following 3 days of treatment. Human tumor cell lines bearing mutations in RAS were highly sensitive to ADT-007 with single digit nanomolar growth inhibition IC_{50} values (**Table 1-Mutant RAS**). Furthermore, tumor cell lines with mutations in *RAS* or upstream signaling components (e.g., RTK or NF1) were equally sensitive to ADT-007 (IC_{50} values in the low nM range, Table 1-RAS pathway activated upstream), while tumor cell lines with WT RAS and downstream MAPK mutations were essentially insensitive to ADT-007 (**Table 1-WT RAS and WT RAS pathway activated downstream**). In addition, cultured cells derived from normal colon (NCM460) or lung (NHAEC) were insensitive to ADT-07 treatment despite being highly proliferative, which we interpret to mean that the cells are not “addicted” to RAS and use other pathways to maintain growth and survival (**Table 1-WT RAS**). Overall, these findings indicate that ADT-007 exhibits true “pan-RAS” inhibitory activity against an array of human tumor cell lines with mutant or hyper-activated WT RAS signaling pathways with no effects on potential by-stander cells.

Among the histologically diverse tumor cell lines evaluated for sensitivity to ADT-007, MIA-PaCa-2 PDAC cells were the most sensitive with IC_{50} values as low as 2 nM with a

selectivity index of ~1200x relative to WT RAS BxPC3 PDAC cells. RAS-RBD pull-down assays confirmed high levels of activated (GTP-bound) RAS among the mutant KRAS PDAC cell lines examined while activated RAS levels in WT RAS BxPC3 cells were essentially undetectable (**Figure 2A**). ADT-007 completely inhibited colony formation of the PDAC cell lines regardless of the KRAS mutation, while RAS WT Bx-PC3 cells were not significantly affected by ADT-007 treatment (**Figure 2B**). As we observed in mutant KRAS mutant CRC cells, ADT-007 selectively induced G2/M (mitotic) arrest in mutant KRAS MIA-PaCa-2 cells, while RAS WT BxPC-3 cells required much higher concentrations of ADT-007 to have the same effect (**Figure 2C**). In addition, ADT-007 induced apoptosis of MIA-PaCa-2 cells as measured by caspase cleavage, although longer durations of treatment were required relative to those required to induce mitotic arrest (**Figure 2D**). ADT-007 resulted in comparable IC_{50} values to reduce viable cell number of MIA-PaCa-2 cells grown in 3-D spheroid cultures as it did in 2-D monolayer cultures (**Figure 2E**). This is significant given that spheroid cultures are known to model the heterogeneity of tumor growth *in vivo* with non-proliferating (necrotic) cells in the core and proliferating cells growing at the periphery of the spheroid (41). Comparable sensitivity of spheroid and monolayer cultures also suggests that the mechanism of cell death by ADT-007 is unrelated to the rate of cell proliferation (e.g., cell doubling time). Another unique characteristic of ADT-007 is an extremely steep dose-response that reflects uniform killing of cancer cells within a narrow dose range and which may be further evidence of a cell cycle independent mechanism of cell death.

Comparison with mutant specific KRAS inhibitors

In a side-by-side comparison, the potency of ADT-007 was measured to be approximately 10x greater than the $KRAS^{G12C}$ inhibitor, AMG-510 (sotorasib) in 3-day growth assays involving $KRAS^{G12C}$ mutant MIA-PaCa-2 cells (**Figure 3A**). Consistent with experiments described above, longer durations of treatment with ADT-007 in colony formation assays (10

days) involving $KRAS^{G12C}$ mutant MIA-PaCa-2 cells resulted in complete inhibition of colony formation at sub-nanomolar concentrations. By comparison, concentrations of AMG-510 at 70 nM were required to have a comparable effect as ADT-007 (**Figure 3B**).

$KRAS^{G12C}$ MIA PaCa-2 cells were continuously cultured with AMG-510 or MRTX-1257 to develop a model of resistance to mutant specific KRAS inhibitors and found to exhibit appreciably higher IC_{50} values to both drugs relative to the parental cell line. By contrast, ADT-007 showed comparable IC_{50} values in the resistant cell lines as the parental MIA PaCa-2 cells (**Figure 3C**).

In addition, Lewis lung cancer cells harboring a $KRAS^{G12C}$ mutation and a secondary mutation in $NRAS^{Q61H}$ were insensitive to AMG-510 but retained high sensitivity to ADT-007 (IC_{50} = 9 nM) (**Figure 3D**). These results suggest that ADT-007 maintains potency in the presence of two independent activating RAS mutations, unlike mutation specific inhibitors, which are known from clinical trials to have modest efficacy or are prone to resistance with acquisition the of additional cis- or trans-mutations in RAS alleles (28-29).

Requirement of activated RAS for sensitivity to ADT-007

The sensitivity of cancer cells with activated RAS to ADT-007 was further studied by transfecting RAS WT HT29 CRC cells with mutant G12C HRAS. Sensitivity to ADT-007 was greatly increased resulting in an IC_{50} of 24 nM compared with 549 nM and 730 nM for parental and vector control HT29 cells, respectively (**Figure 4**). High activated RAS levels were confirmed by RAS-RBD pull-down assays, while parental and vector control HT29 cells with WT RAS had undetectable levels of activated RAS. As another example, transfecting WT RAS BxPC3 PDAC cells with G12C mutant KRAS also increased sensitivity to ADT-007 from 2.5 µM in parental cells to 0.5 µM in KRAS transfected cells (**Figure S1**). A similar induction of

sensitivity to ADT-007 occurred after transfecting RAS WT H322 lung cancer cells with mutant HRAS (data not shown).

The ability of ADT-007 to directly bind RAS in cells was determined using a cellular thermal shift assay (CETSA) as previously described (42). Initial experiments measured the optimal temperature to denature 75% (T_{agg75}) KRAS in lysates followed by western blot (WB) quantification of non-denatured KRAS levels. ADT-007 increased KRAS thermal stability (T_{agg75}) with an EC_{50} of 0.45nM by treating whole cell lysates from mutant $KRAS^{G13D}$ HCT116 cells compared with >1000 nM in WT RAS HT29 cells **(Figure 5)**. ADT-007 did not bind an unrelated protein (PDE10) that was used as a control. In addition, ADT-007 treatment of HEK293 cells transfected with mutant $KRAS^{G12C}$ and probed with anti-Micro-Tag antibody to quantified RAS by WB analysis resulted in an EC_{50} = 8.5 nM that was comparable with growth IC_{50} values (**Figure S2**).

ADT-007 blocks RAS activation and MAPK/AKT signaling

Treatment with ADT-007 in the same concentration range that ADT-007 inhibits growth of mutant KRAS HCT116 cells reduced activated RAS levels as measured by RAS-RBD pull-down assays (**Figure 6**). As further evidence that ADT-007 inhibits activated RAS, the same lysates were probed using phospho-specific antibodies to various downstream signaling components. WB analysis showed that ADT-007 treatment inhibited both RAF/MAPK and PI3K/AKT signaling, which would be expected for a RAS inhibitor. Interestingly, ADT-007 treatment of lysates from KRAS mutant HCT116 cells, G12V HRAS transfected HT29 cells, and G12V HRAS transfected H322 cells also reduced activated RAS levels at concentrations effective for inhibiting the growth of these cell lines (**Figure S3**). These experiments involving the treatment of cell lysates with ADT-007 effectively rules out potential inhibitory effects of ADT-007 on upstream receptor tyrosine kinase signaling components that are active in live cells, but not in cell lysates.

Treatment of KRAS mutant MIA-PaCa-2 cells with ADT-007 also reduced activated RAS levels under multiple growth conditions including cultures grown in the presence of serum, following serum starvation, or following serum starvation and with EGF stimulation (**Figure 7**). As evidence for the chemical and biological specificity of ADT-007, a closely related analog did not reduce activated RAS (data not shown). The pan-RAS inhibitory effect of ADT-007 was confirmed using RAS isozyme specific antibodies (**Figure 8**). These experiments showed that EGF increased levels of activated HRAS and NRAS that were co-expressed with KRAS in KRAS mutant MIA-PaCa-2 PDAC cells. However, EGF did not further activate KRAS as would be expected given that KRAS is already activated by the G12C mutation. As predicted for a pan-RAS inhibitor, ADT-007 blocked EGF activation of WT HRAS and NRAS isozymes, as well as reducing constitutively activated KRAS. These results imply that the co-expression of WT RAS isozymes in KRAS mutant cells could compensate or override the inhibitory effects of a mutant specific KRAS inhibitor to result in resistance (26). The ability of ADT-007 as a pan-RAS inhibitor to block both activated WT and mutant RAS isozymes would reduce the potential for resistance.

ADT-007 treatment of mutant KRAS MIA-PaCa-2 PDAC cells blocked EGF-induced phosphorylation of RAF, MEK, and ERK, as well as AKT as measured using phospho-specific antibodies and probed by WB analysis (**Figure 9**). As a control, the EGFR inhibitor, erlotinib but not ADT-007, blocked EGF phosphorylation of EGFR (data not shown), which is consistent with a direct acting RAS inhibitor. In addition, the MEK inhibitor, U0126, blocked EGF phosphorylation of ERK, but did not affect AKT phosphorylation or upstream RAF or MEK. The MEK inhibitor also caused pathway reactivation, which is a mechanism of resistance to MAPK inhibitors as previously reported (43). Conversely, the PI3K inhibitor LY294002 blocked EGF-induced AKT phosphorylation, but not ERK phosphorylation. ADT-007 also inhibited RAS signaling in MIA PaCa-2 cells under standard cell culture conditions or following serum starvation. Similar inhibitory effects of ADT-007 on RAS-GTP levels and MAPK/AKT signaling

were observed in colon, lung, ovarian, glioma, and melanoma cancer cell lines with mutant KRAS (data not shown). The ability of ADT-007 to concurrently block EGF-stimulated MAPK and AKT pathways further supports a mechanism involving direct inhibition of RAS. Although slightly higher concentrations of ADT-007 were required to inhibit RAS activation and MAPK/AKTsignaling relative to growth IC_{50} values, the difference is likely attributed to the differences in the duration of treatment; overnight for signaling assays vs. 3 days of treatment for growth assays.

ADT-007 binds to nucleotide free KRAS and inhibits loading of GTP

Molecular docking studies using a crystal structure of WT KRAS provided insight as to how ADT-007 may bind RAS (**Figure 10**). Using molecular dynamics followed by Glide docking, a free energy score of -11.1 was calculated for ADT-007 that was comparable to -11.4 for nucleotide (e.g., GDP in this case). Interestingly, the conformation change resulting from ADT-007 binding to RAS dramatically reduced the free energy score of RAS to bind GDP from -11.4 to -7.6 (44).

Recombinant full-length WT KRAS was used to determine if ADT-007 directly binds RAS in a cell-free, reconstituted system. The experiments were designed based on the above molecular docking studies suggesting that ADT-007 preferentially binds RAS when in a nucleotide-free (NF) conformation. GTP binding to RAS was measured using a fluorescent GTP analog (Mant-GTP) (18). Kinetic experiments revealed that ADT-007 reduced the rate of GTP binding to RAS if pretreated with EDTA to chelate Mg^{2+}, which mimics GEF removal of GDP (**Figure 11**), but not if added after adding non-hydrolysable GTPγS. An analog of ADT-007 lacking RAS selective growth inhibitory activity did not alter GTP binding to RAS (data not shown). In addition, a tool compound, CID1067700, previously reported to inhibit GTP binding to

RAS, also inhibited Mant-GTP binding to RAS to a comparable extent as ADT-007 (data not shown) (45).

Other experiments involving recombinant WT RAS and measuring RAS-effector interactions using RAS-RBD pull-down assays revealed that ADT-007 inhibits NF-RAS from binding RAF at growth IC_{50} concentrations, while there was no effect if RAS was preloaded with GTP (**Figure 12**). ADT-007 also blocked RAS-RAF binding using recombinant G12C mutant KRAS under similar experimental conditions (data not shown).

Protein NMR spectroscopy (HSQC) revealed major differences in the spectrum between NF-RAS and GTP-RAS, including signal attenuation at G13, a hotspot mutation site in the P-loop (46), and at K16 (adjacent to S17), which is critical for Mg^{2+} binding (47), as well as shifts or attenuations in signals from other residues (**Figure S4**). ADT-007 caused similar signal attenuation in the G13 and K16 residues (**Figure 13**) along with shifts or attenuations in signals from multiple other residues using NF-RAS **(Figures S5-8)** but did not appreciably affect the NMR spectrum using GTP-RAS (**Figure S9)**. The results support a mechanism by which ADT-007 binds apo-RAS that is known to exist in cells as a transitional state between GDP- and GTP-bound RAS and exerts unique signal transduction activity reported by others (48).

ADT-007 inhibits mouse colon tumor growth and RAS signaling *in vivo*

In order to select the suitable route of administration of ADT-007 in antitumor efficacy studies using mouse models of cancer, the PK profile of ADT-007 was determined after a single treatment by oral (PO), intraperitoneal (IP), and subcutaneous (SC) routes. PK studies revealed that the bioavailability of ADT-007 after PO and SC routes was poor while maximum plasma concentration after IP administration (at 1 hr post treatment) was approximately 100x higher than the tumor growth IC_{50} value (**Figure 14A**). Suspecting that ADT-007 undergoes first-pass metabolism after oral administration, metabolic stability of ADT-007 was evaluated. Evaluation

of ADT-007 glucuronidation was carried out in HT-29 cells reported to express UDP Glucuronidyl Transferase (UGT) activity (49) compared with HCT-116 cells lacking this activity. This showed high levels of ADT-007 glucuronide in HT-29 cells (**Figure 14 B**), paired with dramatically lower intracellular ADT-007 in HT-29 cells than HCT-116 cells (**Figure 14C**). This was further supported by the observations in mouse liver microsome assays which revealed that ADT-007 is vulnerable to glucuronide conjugation by UGT phase II liver metabolism resulting in rapid clearance and excretion (**Figure. 14 D-E**). Prior to addressing this discovered metabolic vulnerability, proof-of-concept *in vivo* experiments were conducted where ADT-007 was administered once daily (QD) by intratumoral (IT) injection to avoid systemic circulation. When administered IT ADT-007 (10 mg/kg, QD) strongly inhibited SC tumor growth (T/C_{max} of 27%) in the KRAS mutant CT26 colon tumor model (**Figure 15A**). To determine if the antitumor activity of ADT-007 was mediated by RAS inhibition, CT26 tumors from mice treated with vehicle or ADT-007 were analyzed by WB analysis for RAS pathway inhibition using phospho-specific antibodies. Treated mice had reduced levels of activated RAS and phosphorylated MAPK components (RAF, MEK, and ERK) compared with control mice (**Figure 15B**).

ADT-007 inhibits growth of human PDAC tumor cells *in vivo* and activates mechanisms of antitumor immunity

We also evaluated the ability of ADT-007 to inhibit growth of patient derived xenograft (PDX) PDAC tumors implanted into NSG mice as a measure of *in vivo* efficacy. Immune deficient, NSG mice engrafted with subcutaneous PDX tumors bearing a codon G12C mutation (PA2) and a codon G12V mutation were treated with peri-tumoral injections of ADT-007 for 2-3 weeks twice daily (BID) and tumor growth was evaluated. In both models, ADT-007 arrested tumor growth in a $KRAS^{G12V}$ (**Figure 16A**) or produced delay of $KRAS^{G12C}$ tumor growth *in vivo* (**Figure 16B**) mutated PDX tumor model.

Next, we assessed the activity of ADT-007 in syngeneic mouse PDAC tumor cell lines bearing $KRAS^{G12D}$ mutation. Cell lines exhibited low IC_{50} values (with the exception of 6419c5) similar to human PDAC cell lines, indicating similar sensitivities of mouse PDAC cell lines to ADT-007 in 2D culture (**Table S1**). Treatment of 2838c3, 7160c2, and 5363 PDAC cell lines with increasing concentrations of ADT-007 inhibited phospho-ERK (data not shown) indicating sensitivity to ADT-007. Intra- or peritumoral administration of ADT-007 into or around subcutaneous CRC CT26 (**Figure 16C**), PDAC 2838c3 (**Figure 16D**), 7160c2 (**Figure 16E**), and 5363 (**Figure 16F**) flank tumors, resulted in significant inhibition of tumor growth in all KRAS mutant tumor models. Antitumor activity of ADT-007 in CT26 tumors was found to be associated with increased helper and cytotoxic T cells, decreased regulatory T cells, and increased pro-inflammatory cytokines (**Figure S10**). Overall, these findings indicate that ADT-007 inhibits growth of human and mouse PDAC (and CRC) tumors *in vivo* and suggests a potential role for tumor immunity in the efficacy of ADT-007 in immune competent recipients.

ADT-007-mediated inhibition of $KRAS^{G12D}$ alters the tumor immune microenvironment

The above findings indicate that ADT-007 inhibits *in vivo* tumor growth of syngeneic G12D mutated CRC and PDAC tumors in both immune deficient and immune competent mouse models. Given the recent publications in preclinical mouse models of colon, lung, and pancreatic cancer, it is clear that targeted mutation specific G12C (22) and G12D inhibitors (25) promote anti-tumor immune responses, which act to control tumor growth. Therefore, we evaluated the impact of the pan-RAS inhibitor ADT-007 on myeloid and T cells in immune competent recipient mice bearing syngeneic mouse 2838c3 and 7160c2 PDAC cell lines using multi-parameter flow cytometry (**Figure S11 and Figure 17**). Both models contain significant numbers of T cells but exhi bit differences in the composition and activation status of T cell subsets, with 2838c3 containing more activated $PD\text{-}1^{+}$ $CD8^{+}$ T cells than 7160c2. Furthermore,

2838c3 has presence of neo-antigens suggesting that the 2838c3 model has greater functional T cell response than 7160c2 (50). At 17 and 21 days of treatment in ADT-007 vs. sham treated 2838c3 and 7160c2 tumor bearing mice, animals were euthanized and tumors collected to evaluate changes in YFP^{+} tumor and $CD11b^{+/-}$ myeloid cell subsets within the TME. In both the 2838c3 and 7160c2 TMEs, ADT-007 decreased the proportion of YFP^{+} tumor cells (**Figure 17A and 17E**) consistent with reductions in tumor weights (data not shown). Within the TiME, ADT-007 treatment resulted in increases in proportions of $CD11b^{+}$ $Ly6G^{+}$ $Ly6C^{+}$ gMDSC and $CD11b^{+}$ $Ly6G^{-}$ $Ly6C^{hi}$ mMDSC subsets in 7160c2, but not 2838c3 tumors (**Figure 17B and 17F**). No significant changes in dendritic cell or macrophage frequencies were noted despite increases in cDC1, cDC2, and $F4/80^{+}$ macrophage subsets in both models. Furthermore, no significant changes in MHCII or CD206 expression were noted in F4/80+ macrophage or dendritic cell subsets (**Figure 17C-D** and **G-H**).

The above findings suggest variable impact of ADT-007 on the percentages and phenotypes of tumor infiltrating myeloid cell subsets was dependent upon the model system. To evaluate the importance of the adaptive immune system in the *in vivo* efficacy of ADT-007, syngeneic mouse PDAC cell lines bearing $KRAS^{G12D}$ 2838c3 and 7160c2 cell lines were implanted into immune competent C57BL/6 mice or C57BL/6 Rag $1^{-/-}$ mice lacking T and B cells. When tumors reached 150 mm^3 mice were treated with peri-tumoral injections of ADT-007 and sham (vehicle) for a period of 17-21 days dependent on tumor growth kinetics. Treatment with ADT-007 reduced growth in both immune competent C57BL/6 and immune deficient C57BL/6 Rag $1^{-/-}$ mice, however, the potency of ADT-007 was reduced in C57BL/6 Rag $1^{-/-}$ recipient mice (**Figure 18A and 18B**) suggesting a role for the adaptive immune response in the *in vivo* efficacy of ADT-007.

To understand the effect of ADT-007 on the adaptive immune response, we evaluated whether ADT-007 treatment altered proportions, activation status, and function of NK and T cell

subsets in the 7160c2 and 2838c3 TiME. Using multi-parameter flow cytometry (**Figure S12**), percentages of NK and T cell subsets were assessed in both models and changes reflected in the % of $CD45^+$ white blood cells. No significant changes in the proportions of $CD3^+$ $CD4^+$ (T_{Helper}), $CD3^+$ $CD4^+$ $Foxp3^+$ (Tregs), $CD3^+$ $CD8^+$ (CTLs), $CD3^+$ $NK1.1^+$ (NKT), $CD3^+$ $TCR\gamma\delta^+$ (γδ T) T , or $CD3^+$ $NK1.1^-$ (NK) cells were noted in the 2838c3 PDAC TiME, although a trend for a decrease in $Foxp3^+$ regulatory T cells was noted in the ADT-007 treated group (**Figure S13A-B**). Significant differences in percentages of some T cell subsets in 7160c2 TiME were noted. ADT-007 treatment decreased percentages of $CD8^+$ T and $NK1.1^+$ NK cells while increasing percentages of γδ T cells (**Figure 18C+D**). These findings indicate that a 21-day treatment course of ADT-007 modulates proportions of T cells in the 7160c2 TiME. Next, we evaluated the activation status of T cell subsets by expression of CD44 and CD62L to identify the proportions of naïve ($CD62L^+$ $CD44^-$), pre-effector ($CD62L^-$ $CD44^-$), effector memory ($CD62L^-$ $CD44^{hi}$), and central memory ($CD62L^+$ $CD44^{hi}$) T cells within each subset. ADT-007 treatment did not significantly impact activation of T cell subsets in the 2838c3 TME except for the γδ T cells, which exhibited a $CD44^{hi}$ $CD62L^-$ effector memory phenotype (**Figure S13C+D**). In comparison, T cell phenotypes in the 7160c2 TME shifted to a $CD44^{hi}$ $CD62L^-$effector memory phenotype with ADT-007 treatment (**Figure 18E**) indicating that ADT-007 induced effector memory T cells in the 7160c2 TiME.

No differences were noted in the sensitivity of 2838c3 and 7160c2 to ADT-007 (3.7 vs. 1.65 nM respectively, data not shown), suggesting that these differences in T cell infiltration and activation were not a result of the impact of ADT-007 on oncogenic RAS inhibition in each PDAC tumor model. Instead, these findings suggest that intrinsic differences in the PDAC tumor microenvironment influence the magnitude and nature of the immune response elicited by the pan-RAS inhibitor ADT-007. A potential concern in use of a pan-RAS inhibitor, is the potential off target impact on WT RAS-MAPK signaling in metabolically active cells, like activated T or B

cells; however, the ability of ADT-007 to either have no impact or enhance effector T cell phenotypes in the PDAC TiME suggests that this is unlikely.

Lastly, we evaluated the impact of ADT-007 on the function of tumor infiltrating NK and T cell subsets in 2838c3 and 7160c2 tumor models. To do this, production of IL-2, IFNγ, TNFα, and Granzyme B in T cell subsets were assessed by intracellular staining after PMA and ionomycin stimulation in the presence of brefeldin A. In the 7160c2 TiME both $CD4^+$ and $CD8^+$ T cells exhibited increased production of IL-2, Granzyme B, IFNγ, and TNFα (**Figure 18F-H**); whereas minimal changes in cytokine expression were noted in T cells within the 2838c3 TiME (**Figure S13 E-F**). Effector activity of NK and T cells were further evaluated using an IFNγ-Thy1.1 reporter model system (51) (52), where induction of IFNγ results in expression of surface Thy1.1 providing the ability to trace history and active IFNγ production through surface expression of Thy1.1. Using this model, we evaluated the impact of ADT-007 on IFNγ production history of NK and T cell subsets in both the 2838c3 and 7160c2 TiME. Consistent with ICS findings, ADT-007 had minimal impact on IFNγ production with exception of NK cells, which had reduced Thy1.1 expression compared to sham treatment (**Figure S14A-B**) in both the 2838c3 and 7160c2TiME, whereas CD4 and CD8 T cells exhibited increased production of IFNγ *in vivo* in the 7160c2 TiME (**Figure S14B**). Interestingly Thy1.1 expression was significantly reduced in $CD4^+$ $Foxp3^+$ regulatory T cells in 7160c2, but not 2838c3 TiME indicating a reduction of IFNγ production by regulatory T cells (**Figure S14B**). Overall, these findings suggest that pan-RAS inhibitors have the ability to modulate tumor immunity, but responses are variable and likely dependent on the composition, genetics, and function of tumor, stroma, and immune cells within the TME.

Discussion:

These findings indicate that ADT-007 is a highly potent pan-RAS inhibitor specific for the nucleotide free, apoenzyme state of RAS and inhibits downstream MAPK and PI3K signaling in KRAS-addicted tumors. ADT-007 induces growth arrest and/or tumor regression in human xenograft models in immunodeficient mice and syngeneic mouse CRC and PDAC tumor models with a partial dependence on the adaptive immune system. ADT-007 activated T cells and enhanced their cytotoxic functions in some of the $KRAS^{G12D}$ mutated CRC and PDAC tumor models tested. Overall, these findings indicate that the novel pan-RAS inhibitor ADT-007 is a potent and selective inhibitor for mutated and WT KRAS addicted tumors with *in vivo* potency and evidence of immune modulation in both pancreatic and colorectal cancer. The potency, immune modulatory potential, and ability to inhibit all RAS mutations with the pan-RAS inhibitor ADT-007 provides a novel therapeutic with the potential to be used as 1st or 2nd line therapy alone or in sequence with mutation specific RAS inhibitors.

ADT-007 pan-RAS specificity for the nucleotide free apoenzyme

ADT-007 exhibits novel binding to nucleotide free apoRAS confirmed by biochemical studies including cellular thermal shift assays, NMR spectroscopy, RAS-RAF pull-down assays using EDTA-chelated nf KRAS to mimic the apoenzyme state. Under normal steady state, a small fraction of RAS exists in the apoenzyme state, which can be a target for inhibition of mutant KRAS activation as demonstrated with RAS apo-enzyme-specific antibodies that inhibit GTP-loading and activation of downstream signaling through MAPK and PI3K pathways (53). Unlike targeted or KRAS selective inhibitors (54) (21), ADT-007 exhibits broad specificity for mutant K/H/NRAS isozymes to inhibit downstream MAPK and PI3K signaling critical for growth and survival of cancer cells that exhibit intrinsic, mutation-specific or extrinsic wild type RAS addiction.

ADT-007 inhibits a wide range of RAS-addicted tumors and circumvents resistance involving reactivation of the RAS pathway

Given the broad specificity of this inhibitor, it provides a potentially generalizable therapeutic for patients with PDAC as 94% of patients with this disease have KRAS mutations (30) and a significant proportion of patients with WT KRAS have RTK fusions that would be predicted to hyper-activate WT KRAS (55). Furthermore, evidence indicates that ADT-007 exhibits greater potency in tumor cells with higher levels of active RAS signaling, which may provide greater therapeutic utility in patients with metastatic disease, which is dependent upon enhanced oncogenic KRAS signaling for proliferation in the metastatic niche (56) (57). ADT-007 exhibits potent growth inhibition *in vitro* and *in vivo* with syngeneic $KRAS^{G12D}$ mutated CRC and PDAC cell lines and human $KRAS^{G12C}$ and $KRAS^{G12V}$ mutated PDAC PDX models consistent with pan-RAS inhibitory activity. Additional work across a more diverse spectrum of RAS mutant and hyper-activated human tumor cell lines and PDX model systems will be needed to better extrapolate the potency of ADT-007 in CRC and PDAC patients.

Equally important, is that this broad specificity has the potential to provide a second line therapy for patients that develop resistance to mutation-specific inhibitors. In NSCLC patients who go on to develop resistance to G12C specific KRAS inhibitors, the majority of resistance pathways involve further modulation of RAS signaling including polyclonal mutations in RAS or upstream receptor tyrosine kinases or GTPase that result in dysregulated WT RAS signaling (58) (28). Our *in vitro* findings indicate that ADT-007 maintains potency and growth inhibition in MIA Paca-2 cell lines that develop resistance to Sotorasib and Adagrasib (59) or LLC lines with $KRAS^{G12C}$ $NRAS^{Q61H}$ dual mutations (60).

ADT-007 modulates the tumor immune microenvironment

ADT-007-mediated *in vivo* tumor growth-inhibition appears to be partially dependent upon the adaptive immune response as evidenced by reduced growth inhibitory activity of ADT-007 in immune deficient Rag $1^{-/-}$ mice lacking B and T cells. Similar findings have been noted

with G12C (22) (24) and G12D-specific inhibitors (25), which demonstrated that T cells are important for response to targeted mutation-specific KRAS inhibitors and long-term control of regrowth of 2838c3 PDAC tumors treated with the $KRAS^{G12D}$ inhibitor MRTX-1133 (25). Furthermore, the presence of T cells predicted the response to PD-1 immune checkpoint blockade (24). Despite this dependency the impact of ADT-007 mediated inhibition of oncogenic $KRAS^{G12D}$ signaling, the impact on T cell numbers, activation, and function was variable and dependent upon the model system. In both CT26 and 7160c2 tumor models, ADT-007 treatment enhanced priming, activation, and functions of T cell subsets resulting in increased production of T_H1 cytokines including IL-2, TNFα, IFNγ, and the cytotoxic protein granzyme B. This was not observed in the 2838c3 model, in which T cell proportions, activation, and function were largely unaffected despite trends for increase in granzyme B and polyfunctional IL-2^+ IFNg^+ Granzyme B^+ T cells (data not shown). It is clear that diversity within KPC tumor clones, in part through epigenetic patterns of tumor behavior, in turn influences the composition and function of immune cells in the TME (50). Therefore, it is likely that myeloid and T cell responses will vary among preclinical tumor models due to variations in tumor biology that impact the local immune microenvironment (25) (24).

A significant concern in this study was the impact of the pan-RAS inhibitor on RAS-MAPK signaling in tumor infiltrating lymphocytes, specifically cytotoxic NK and T cell subsets. Previous genetic studies evaluating the role of RAS signaling in T cell development revealed a role for RAS isozymes in thymic selection, T_H1 T, and NK cell function (61) (62) (63) (64) (65). In 2838c3 and 7160c2 PDAC models, no significant impairment of IFNγ production was noted in T cell subsets isolated from either TME suggesting that the local (peritumoral) inoculation of the pan-RAS inhibitor ADT-007 did not significantly impair cytokine production by tumor infiltrating T cell subsets (CD4, CD8, NKT, γδ T cells) or the importance of adaptive immunity in drug efficacy. In contrast, IFNγ production from tumor infiltrating NK cells was decreased in both models suggesting a potential impairment of NK cell activity with peritumoral administration of

ADT-007. Previous studies demonstrated a role for RAS signaling in the ability of human NK cells to produce IFNγ in response to *in vitro* mitogenic stimulation, suggesting a role for RAS-signaling in NK cell function (61). Inter-model and temporal variability in the tumor immune response was noted in response to the G12D-specific inhibitor MRTX-133, however, long-term control of tumor growth after discontinuing MRTX-133 was critically dependent upon T cells indicating a role for T cells in restraining tumor growth (25). Overall, these and previous studies in preclinical NSCLC and PDAC models indicate that the presence of T cells is important to the efficacy of targeted RAS inhibition through either mutation-specific or pan-RAS inhibitors and that the presence of functional T cells is critical for synergistic activity between targeted RAS inhibition and immune checkpoint blockade (22) (24).

Summary

ADT-007 is a potent, pan-RAS inhibitor specific for apo-RAS isozymes that demonstrates *in vivo* efficacy with a variety of different KRAS mutated human and mouse models of colorectal and pancreatic cancer. ADT-007 maintains efficacy *in vitro* in tumor cell lines that exhibit resistance to G1C inhibitors and tumor cell lines with multiple mutations in RAS. We also demonstrate that ADT-007 modulates tumor immune responses. We hypothesize that ADT-007 provides a novel treatment that is generalizable to benefit patients with RAS mutated or addicted tumors and provides a means to specifically target patients who develop RAS-dependent mechanisms of resistance to mutant specific KRAS inhibitors.

Material and Methods:

Mice: 8 week-old female C57BL/6 mice (000664), female **B6.129S7-*Rag1*^{tm1Mom}/J (002216)** male and female NOD.Cg-*Prkdc*^{scid} *Il2rg*^{tm1Wjl}/SzJ (NSG, 00557) were purchased from Jackson Laboratory. 7-weel-old female BALB/c mice (028) and *nu/nu* nude mice (088) were purchased from Charles River Laboratories. B6.Ifng/Thy1.1 KI (IFN-γ.Thy1.1) and B6.Cg-Tg-IL2$^{tm1(eGFP)/Weav}$ (IL-2.GFP) knock-in cytokine reporter mice were kindly provided by Dr. Casey Weaver (University of Alabama at Birmingham, Birmingham, AL) (52). Experiments were randomized, but not blinded. All animal experiments and procedures were performed under approved protocols in accordance with guidelines from the University's Institutional Animal Care & Use Committee (IACUC).

Cell lines: Murine PDAC cell lines were derived from tumor-bearing KPC/Y mice (7160c2, 2838c3) (50). Cells were cultured in Dulbecco's Modified Eagle Medium DMEM (high 440 glucose without sodium pyruvate) supplemented with 10% heat-inactivated fetal bovine serum (FBS), and 1% penicillin/streptomycin. Human PDAC cell lines (BxPC-3, CFPAC-1, MIA Paca-2, Panc-1, SW-1990), CRC (human HT29, HT116, and murine CT-26) cell lines, and murine Lewis lung carcinoma cell line were purchased from ATCC and maintained according to ATCC guidelines. All cell lines were tested against an extended panel of excluded pathogens including mycoplasma prior to *in vivo* studies as mandated by institutional animal resources program (ARP) and IACUC guidelines.

Spheroid Cell Culture: Human MiaPaca-2 cell lines were seeded at a density of 10^3 to 1.5 x 10^3 cells into single wells of 96 well cell culture plates coated with a 1.5% agarose. Cells were cultured for 72 hours then 50% of the media was replaced with either media containing vehicle (DMSO at 1%) or increasing concentrations of ADT-007 (0.1, 0.5, 1, 5, 10, 50, 100, 1000nM) for up to 10 days. Cells were then dissociated and cell numbers were enumerated andIC_{50} calculated.

Tumor cell transfections: BxPC3 cells were initially exposed to lentiviral particles containing a mutant HA-*KRAS* G12C construct for 48 hours in a 6-well plate at 37°C in a humidified incubator with 5% carbon dioxide. The media was then removed and replenished with fresh media containing HA-*KRAS* G12C lentiviral particles. After another 48 hours, the media was removed, and fresh media containing 5 µg/mL puromycin was added to the well. Surviving cells were expanded in a 10 cm dish, and expression of the construct was confirmed by WB with an HA tag antibody (Cell Signaling Technology).*In vitro* stimulation and ADT-007 treatments: For *in vitro* ADT-007 studies 2D and 3D cell cultures were incubated with increasing concentrations (0.1, 0.5, 1, 5, 10, 50, 100, 250, 500, 1000, 10000 nM) of ADT-007, AMG-510 (Selelck Chemicals, Houston, TX) or MRTX849 (Selleck Chemicals, Houston, TX) . or vehicle (DMSO) for a period of 24 – 72 hours depending on the assay. In some experiments 10 ng of recombinant, mouse EGF (Gibco, Jenks, OK) was added 10 minutes prior to harvesting protein lysates from treated tumor cell lines to assess the impact of upstream receptor tyrosine kinase signaling on RAS-MAPK and RAS-PI3K pathways.

Cell growth assays: To determine IC_{50} values, 5 x 10^3 tumor cells were plated in triplicate in 96 well flat bottom plate and incubated with various concentrations of ADT-007 (0.1. 0.5. 1, 5, 10, 50, 100, 250, 500, 1000, 10000 nM) and cultured for a 72-96 hour period depending on cellular growth kinetics. At 72 hours, cells were processed according to the manufacturer's recommendations to assess intra-cellular ATP levels as a measure of cellular proliferation and viability. Cell viability was read 72 hours later using CellTiter-Glo (Promega, Madison, WI) according to manufacturer's instructions. Curves showing the effects of compound concentration on colony count were generated using GraphPad Prism.

Colony formation assays: Approximately 500 cells/well (6-well plate) were incubated for 24 hours at 37°, dosed the 24 hours later with either increasing concentrations of ADT-007 (0.5. 5, 20, 30, 40, 50, 70 nM), AMG-510 (0.5. 5, 20, 30, 40, 50, 70 nM), or DMSO and then incubated

for period of 10-14 days. Endpoints were determined when colonies in the vehicle control wells reached a size of approximately 50 cells or larger. At endpoint, wells were washed in PBS, then stained for 1 hour at RT in 2 mL of crystal violet solution in 1% formalin and 1% methanol. Plates were imaged using a ChemiDoc Imaging System (Bio-Rad, Hercules, CA), and colonies were counted using a custom macro in Nikon Elements Research developed by Dr. Joel Andrews (University of South Alabama).

NMR Spectroscopy: Recombinant WT KRAS in was dialyzed twice for 24 hours (12 hours each time against 1 L of 50 mM Tris-Citrate pH=6.5, 50 mM NaCl, 10 mM β-mercaptoethanol) at 4 ºC following treatment with 10 mM EDTA to remove Mg^{2+} and the bound nucleotide. To record ^{1}H-^{15}N heteronuclear single quantum coherence (HSQC) NMR spectra of nfKRAS we used 900 MHz and 600 MHz Avance spectrometers (Bruker, Billerica, MA, USA), equipped with cryogenic probes. Each *in vitro* experiment was performed at 25°C in 50 mM Tris-Citrate pH=6.5, 50 mM NaCl, 10 mM β-mercaptoethanol containing 10% $^{2}H_2O$. The chemical shift assignments were taken from the Biological Magnetic Resonance Data Bank (BMRB) database (http://www.bmrb.wisc.edu) by use of the BMRB accession numbers: 18529, 25114, and 26635.

$$\Delta\delta_{NH} = \sqrt{\frac{(\Delta\delta^{1}H_N)^2 + (\frac{\Delta\delta^{15}N)^2}{25}}{2}}$$

Chemical shift perturbations (CSPs) higher than the sum of the average and 1 SD were considered to be statistically significant.

Nucleotide Exchange Assays: The fluorescent GTP analog MANT-GTP was purchased from Millipore Sigma. For each reaction, 5 µL of 5 µM purified GDP-bound K-RAS in reaction buffer (40 mM Tris-HCl, 100 mM NaCl, 20 mM MgCl, 1 mg/mL BSA, pH 7.5) and 2.5 µL of 200 mM EDTA was added to a microcentrifuge tube to make a master mix. Water was used in place of EDTA in some reactions as a control for the release of GDP. 7.5 µL of master mix per well was

added to a 384-well plate for each respective reaction. 5 µL of compound at five times the desired concentration or vehicle in reaction buffer was added to each respective well. After 2.5 minutes for equilibration at 26°C in a Bio-Tek Synergy H4 microplate reader, 12.5 µL of 1.5 µM MANT-GTP in reaction buffer was added to each well for a final concentration of 750 nM MANT-GTP, 1 µM RAS, 20 mM EDTA, and the desired concentration of compound or vehicle. In the case of compound preincubation, the plate was incubated for 1 hour at 26°C prior to MANT-GTP addition. Fluorescence was measured at an excitation wavelength of 360 nm and an emission wavelength of 460 nm in a Bio-Tek Synergy H4 microplate reader. Kinetic curves were generated with GraphPad Prism.

Cellular Thermal Shift Assay: The Micro-tag in-cell binding assay was performed using the NERD BIO Micro-Tag enzyme complementation method. A KRAS G12C Micro-Tag construct was engineered having a 15-amino acid tag at the N-terminus. The construct was transiently expressed in HEK293 cells. Two days post-transfection cells were lifted, washed with Tris Buffered Saline (TBS: 20mM Tris HCl pH7.4, 150mM NaCl) and re-suspended at 1000 cells/µl in TBS and 50,000 cells aliquoted to wells of a PCR plate. Increasing doses of compounds were added and incubated with cells for 45min followed by heating for 10min at 55°C and a 1min cool down on ice. An equal volume of 0.5% Triton-X-100 in TBS was added, and cells lysed for 10min on ice followed by addition of the Tag binding protein and substrate and immediately proceeded to measurement of fluorescence signal. Fluorescence signal was plotted with concentration of the compounds on a semi-log scale using GraphPad Prism 9.0 software. Non-linear regression analysis was used to fit a Sigmoidal dose-response curve with variable slope to generate EC_{50} values for in-cell target engagement for the compounds.

Western blotting: Tumor lysates were generated after treatment with 500 uL RIPA lysis buffer (e.g. Thermo Scientific, 89900) with protease and phosphatase inhibitors (e.g. Thermo

Scientific, 78443), boiled for 5 minutes and equal protein concentrations were loaded and run on a 12% SDS-PAGE. Gels were transferred to a PVDF membrane, which were blocked with either 5% non-fat dry milk in TBS-T (TBS with 0.1% Tween 20) or 5% BSA in TBS-T, depending on the blocking agent used for the primary antibodies, for 1 hour at room temperature. Membranes were incubated overnight at 4°C on a rocker with primary antibodies **(Table S2**) according to the manufacturer's instructionsand then developed with HRP-conjugated secondary antibodies (Cell Signaling Technology) for 1 hour at room temperature on an orbital shaker. Membranes were developed using SuperSignal West Enhanced Chemiluminescent substrate (Thermo Fisher Scientific) and imaged using a ChemiDoc Imaging System (Bio-Rad).

Tumor cell implantation and ADT-007 treatment: A single cell suspension of murine CRC or PDAC cells was prepared PBS and kept on ice until injection. $1x10^6$ syngeneic mouse CRC and PDAC tumor cells were injected subcutaneously into 6–8-week-old BALB/C or C57BL/6 mice respectively. When tumors reached an average tumor volume of 150 mm^3 mice began receiving daily intra-tumoral (10 mg/kg, QD, 7 days/week for 17-21 days) or peri-tumoral (5 mg/kg, BID, 7 days/week for 17-21 days). Tumor growth was assessed by caliper measurements (2-3/week) and tumor volumes ($TV = W \times L^2/2$) were calculated throughout the study. No overt signs of toxicity (body weight loss or organ [lungs, heart, liver, GI tract] pathology) were noted with local administration.

Flow Cytometry: Mouse tumors were digested in a 1 mg/mL collagenase IV and 0.1 mg/mL DNSase 1 (Worthington Biochemical, Lakewood, NJ) in HBSS for 45 minutes at 37 °C with intermittent shaking. Samples were then washed with RPMI containing 10% FBS and filtered through a 70μM strainer generating single cell suspensions. Cells were labeled with primary fluorophore-conjugated antibodies and a live/dead stain (**Table S3**) for 30-60 min at 4 °C, washed and re-suspended in flow buffer. Cytokine expression from single cell suspensions of spleen and tumor was quantified as follows: cells were plated at a concentration of 10^6 cells in 1

mL of RP-10 media and stimulated for 5 hours at 37°C using a 1x solution of a Cell Activation Cocktail containing PMA ionomycin, and Brefeldin A (Biolegend, San Diego, CA). Conversely, cells were cultured for 5 hours at 37°C using using a solution containing 5 ug of Brefeldin A (BioLegend, San Diego, CA) to serve as an unstimulated control. After cell surface staining, cells were fixed in 4% paraformaldehyde for 45 minutes at 4 °C then washed with 1x Perm/Wash (BD, 554723). For intracellular staining in tumor and spleen samples, cells were stained with an antibody cocktail specific intracellular cytokines (IL-2, IFNγ, TNFα, and granzyme B) in Perm/Wash solution for 60 minutes at 4 °C. Data were acquired on a Symphony A5 flow cytometer, with analysis performed using FlowJo version 10.7.2.

Annexin V Assays: Approximately 10^6 HCT116 and HT29 cell lines were cultured in 6-well plates containing DMEM complete media with increasing concentrations of ADT-007 [] or sham (DMSO) for 72 hours. Cells were trypsinized and then stained with 5 uL of Annexin V alexa flour 488 (ThermoFisher, A13201) according to manufacturer's instructions. Cells were analyzed on BD Symphony A5 flow cytometer and data was analyzed using FlowJo version 10.7.2.

Histology: Tissues were fixed overnight in 10% neutral buffered formalin. Tissues were sectioned at 5uM. Hematoxylin & Eosin and Masson's Trichrome stains were performed according to protocols established by the Comparative Pathology Lab (UAB, ARP).

PI Cell Cycle Analysis: 10^6 HCT116 and HT29 tumor cells were cultured in DMEM complete media containing increasing concentrations of ADT-007 [0, 0.5, 1, 5, 10, 20 nM] or Vehicle (DMSO) for 24 hours. Cells were trypsinized and then fixed in ice-cold 70% EtOH for 1 hour at 4°C. After fixation/permeabilization cells were incubated in 500 uL of PI cell cycle buffer containing RNAse (BD, 550825) for 15 minutes prior to flow cytometry acquisition using BD Symphony A5 flow cytometer. Cells were acquired in the linear scale and doublets excluded using FL3 area vs FL3 height parameters and samples were run through FlowJo version 10.7.2,

specifically using its cell cycle analysis application to best fit and evaluate percentages of cells subG0, G1/0, S, G2, and mitotic phases.

Statistical Analyses: GraphPad Prism (version 9.1.2) was used for statistical analyses and graphical representation with data are presented as either means ± standard deviation (SD) or standard error of the mean (SEM). Two-tailed Student's t-test and Two-way ANOVA with multiple corrections (Bonnferoni method) were performed for determination of statistical significance between groups. For IC_{50} generation, concentrations were log transformed, data were then normalized to control and *log*(inhibitor) vs. response (three parameters) test was used. A $p < 0.05$ was considered statistically significant.

References:

1. Siegel RL, Miller KD, Fuchs HE, Jemal A. Cancer statistics, 2022. CA Cancer J Clin. 2022;72(1):7-33.
2. Yang Y, Zhang H, Huang S, Chu Q. KRAS Mutations in Solid Tumors: Characteristics, Current Therapeutic Strategy, and Potential Treatment Exploration. J Clin Med. 2023;12(2).
3. Hingorani SR, Petricoin EF, Maitra A, Rajapakse V, King C, Jacobetz MA, et al. Preinvasive and invasive ductal pancreatic cancer and its early detection in the mouse. Cancer Cell. 2003;4(6):437-50.
4. Kojima K, Vickers SM, Adsay NV, Jhala NC, Kim HG, Schoeb TR, et al. Inactivation of Smad4 accelerates Kras(G12D)-mediated pancreatic neoplasia. Cancer Res. 2007;67(17):8121-30.
5. Bardeesy N, Aguirre AJ, Chu GC, Cheng KH, Lopez LV, Hezel AF, et al. Both p16(Ink4a) and the p19(Arf)-p53 pathway constrain progression of pancreatic adenocarcinoma in the mouse. Proc Natl Acad Sci U S A. 2006;103(15):5947-52.
6. Ying H, Kimmelman AC, Lyssiotis CA, Hua S, Chu GC, Fletcher-Sananikone E, et al. Oncogenic Kras maintains pancreatic tumors through regulation of anabolic glucose metabolism. Cell. 2012;149(3):656-70.
7. Mukhopadhyay S, Goswami D, Adiseshaiah PP, Burgan W, Yi M, Guerin TM, et al. Undermining Glutaminolysis Bolsters Chemotherapy While NRF2 Promotes Chemoresistance in KRAS-Driven Pancreatic Cancers. Cancer Res. 2020;80(8):1630-43.
8. Collins MA, Brisset JC, Zhang Y, Bednar F, Pierre J, Heist KA, et al. Metastatic pancreatic cancer is dependent on oncogenic Kras in mice. PLoS One. 2012;7(12):e49707.
9. Boutin AT, Liao WT, Wang M, Hwang SS, Karpinets TV, Cheung H, et al. Oncogenic Kras drives invasion and maintains metastases in colorectal cancer. Genes Dev. 2017;31(4):370-82.
10. Zhang Y, Yan W, Collins MA, Bednar F, Rakshit S, Zetter BR, et al. Interleukin-6 is required for pancreatic cancer progression by promoting MAPK signaling activation and oxidative stress resistance. Cancer Res. 2013;73(20):6359-74.
11. Ancrile B, Lim KH, Counter CM. Oncogenic Ras-induced secretion of IL6 is required for tumorigenesis. Genes Dev. 2007;21(14):1714-9.
12. Sparmann A, Bar-Sagi D. Ras-induced interleukin-8 expression plays a critical role in tumor growth and angiogenesis. Cancer Cell. 2004;6(5):447-58.
13. Zdanov S, Mandapathil M, Abu Eid R, Adamson-Fadeyi S, Wilson W, Qian J, et al. Mutant KRAS Conversion of Conventional T Cells into Regulatory T Cells. Cancer Immunol Res. 2016;4(4):354-65.
14. Pylayeva-Gupta Y, Lee KE, Hajdu CH, Miller G, Bar-Sagi D. Oncogenic Kras-induced GM-CSF production promotes the development of pancreatic neoplasia. Cancer Cell. 2012;21(6):836-47.
15. Bayne LJ, Beatty GL, Jhala N, Clark CE, Rhim AD, Stanger BZ, et al. Tumor-derived granulocyte-macrophage colony-stimulating factor regulates myeloid inflammation and T cell immunity in pancreatic cancer. Cancer Cell. 2012;21(6):822-35.
16. Ischenko I, D'Amico S, Rao M, Li J, Hayman MJ, Powers S, et al. KRAS drives immune evasion in a genetic model of pancreatic cancer. Nat Commun. 2021;12(1):1482.
17. Coelho MA, de Carne Trecesson S, Rana S, Zecchin D, Moore C, Molina-Arcas M, et al. Oncogenic RAS Signaling Promotes Tumor Immunoresistance by Stabilizing PD-L1 mRNA. Immunity. 2017;47(6):1083-99 e6.
18. Glorieux C, Xia X, He YQ, Hu Y, Cremer K, Robert A, et al. Regulation of PD-L1 expression in K-ras-driven cancers through ROS-mediated FGFR1 signaling. Redox Biol. 2021;38:101780.

19. Muthalagu N, Monteverde T, Raffo-Iraolagoitia X, Wiesheu R, Whyte D, Hedley A, et al. Repression of the Type I Interferon Pathway Underlies MYC- and KRAS-Dependent Evasion of NK and B Cells in Pancreatic Ductal Adenocarcinoma. Cancer Discov. 2020;10(6):872-87.
20. Stalnecker CA, Der CJ. RAS, wanted dead or alive: Advances in targeting RAS mutant cancers. Sci Signal. 2020;13(624).
21. Kwan AK, Piazza GA, Keeton AB, Leite CA. The path to the clinic: a comprehensive review on direct KRAS(G12C) inhibitors. J Exp Clin Cancer Res. 2022;41(1):27.
22. Canon J, Rex K, Saiki AY, Mohr C, Cooke K, Bagal D, et al. The clinical KRAS(G12C) inhibitor AMG 510 drives anti-tumour immunity. Nature. 2019;575(7781):217-23.
23. Briere DM, Li S, Calinisan A, Sudhakar N, Aranda R, Hargis L, et al. The KRAS(G12C) Inhibitor MRTX849 Reconditions the Tumor Immune Microenvironment and Sensitizes Tumors to Checkpoint Inhibitor Therapy. Mol Cancer Ther. 2021;20(6):975-85.
24. Mugarza E, van Maldegem F, Boumelha J, Moore C, Rana S, Llorian Sopena M, et al. Therapeutic KRAS(G12C) inhibition drives effective interferon-mediated antitumor immunity in immunogenic lung cancers. Sci Adv. 2022;8(29):eabm8780.
25. Kemp SB, Cheng N, Markosyan N, Sor R, Kim IK, Hallin J, et al. Efficacy of a Small-Molecule Inhibitor of KrasG12D in Immunocompetent Models of Pancreatic Cancer. Cancer Discov. 2023;13(2):298-311.
26. Ryan MB, Fece de la Cruz F, Phat S, Myers DT, Wong E, Shahzade HA, et al. Vertical Pathway Inhibition Overcomes Adaptive Feedback Resistance to KRAS(G12C) Inhibition. Clin Cancer Res. 2020;26(7):1633-43.
27. Tanaka N, Lin JJ, Li C, Ryan MB, Zhang J, Kiedrowski LA, et al. Clinical Acquired Resistance to KRAS(G12C) Inhibition through a Novel KRAS Switch-II Pocket Mutation and Polyclonal Alterations Converging on RAS-MAPK Reactivation. Cancer Discov. 2021;11(8):1913-22.
28. Awad MM, Liu S, Rybkin, II, Arbour KC, Dilly J, Zhu VW, et al. Acquired Resistance to KRAS(G12C) Inhibition in Cancer. N Engl J Med. 2021;384(25):2382-93.
29. Dunnett-Kane V, Nicola P, Blackhall F, Lindsay C. Mechanisms of Resistance to KRAS(G12C) Inhibitors. Cancers (Basel). 2021;13(1).
30. Waters AM, Der CJ. KRAS: The Critical Driver and Therapeutic Target for Pancreatic Cancer. Cold Spring Harb Perspect Med. 2018;8(9).
31. Piazza GA, Alberts DS, Hixson LJ, Paranka NS, Li H, Finn T, et al. Sulindac sulfone inhibits azoxymethane-induced colon carcinogenesis in rats without reducing prostaglandin levels. Cancer Res. 1997;57(14):2909-15.
32. Piazza GA, Rahm AK, Finn TS, Fryer BH, Li H, Stoumen AL, et al. Apoptosis primarily accounts for the growth-inhibitory properties of sulindac metabolites and involves a mechanism that is independent of cyclooxygenase inhibition, cell cycle arrest, and p53 induction. Cancer Res. 1997;57(12):2452-9.
33. Gurpinar E, Grizzle WE, Piazza GA. NSAIDs inhibit tumorigenesis, but how? Clinical cancer research : an official journal of the American Association for Cancer Research. 2014;20(5):1104-13.
34. Xiao D, Deguchi A, Gundersen GG, Oehlen B, Arnold L, Weinstein IB. The sulindac derivatives OSI-461, OSIP486823, and OSIP487703 arrest colon cancer cells in mitosis by causing microtubule depolymerization. Mol Cancer Ther. 2006;5(1):60-7.
35. Herrmann C, Block C, Geisen C, Haas K, Weber C, Winde G, et al. Sulindac sulfide inhibits Ras signaling. Oncogene. 1998;17(14):1769-76.
36. Karaguni IM, Glusenkamp KH, Langerak A, Geisen C, Ullrich V, Winde G, et al. New indene-derivatives with anti-proliferative properties. Bioorg Med Chem Lett. 2002;12(4):709-13.
37. Gala M, Sun R, Yang VW. Inhibition of cell transformation by sulindac sulfide is confined to specific oncogenic pathways. Cancer Lett. 2002;175(1):89-94.

38. Thompson HJ, Briggs S, Paranka NS, Piazza GA, Brendel K, Gross PH, et al. Inhibition of mammary carcinogenesis in rats by sulfone metabolite of sulindac. Journal of the National Cancer Institute. 1995;87(16):1259-60.
39. Karaguni IM, Herter P, Debruyne P, Chtarbova S, Kasprzynski A, Herbrand U, et al. The new sulindac derivative IND 12 reverses Ras-induced cell transformation. Cancer Res. 2002;62(6):1718-23.
40. Xiao Z, Xue J, Semizarov D, Sowin TJ, Rosenberg SH, Zhang H. Novel indication for cancer therapy: Chk1 inhibition sensitizes tumor cells to antimitotics. Int J Cancer. 2005;115(4):528-38.
41. Daster S, Amatruda N, Calabrese D, Ivanek R, Turrini E, Droeser RA, et al. Induction of hypoxia and necrosis in multicellular tumor spheroids is associated with resistance to chemotherapy treatment. Oncotarget. 2017;8(1):1725-36.
42. Her NG, Babic I, Yenugonda VM, Kesari S, Nurmemmedov E. Cellular thermal shift analysis for interrogation of CRISPR-assisted proteomic changes. Biotechniques. 2020;68(4):180-4.
43. Turke AB, Song Y, Costa C, Cook R, Arteaga CL, Asara JM, et al. MEK inhibition leads to PI3K/AKT activation by relieving a negative feedback on ERBB receptors. Cancer Res. 2012;72(13):3228-37.
44. Desmond Molecular Dynamics System New York, NY: D.E. Shaw Research; 2021 [Available from: https://www.deshawresearch.com/downloads/download_desmond.cgi/.
45. Agola JO, Hong L, Surviladze Z, Ursu O, Waller A, Strouse JJ, et al. A competitive nucleotide binding inhibitor: in vitro characterization of Rab7 GTPase inhibition. ACS Chem Biol. 2012;7(6):1095-108.
46. Hunter JC, Manandhar A, Carrasco MA, Gurbani D, Gondi S, Westover KD. Biochemical and Structural Analysis of Common Cancer-Associated KRAS Mutations. Molecular cancer research : MCR. 2015;13(9):1325-35.
47. John J, Rensland H, Schlichting I, Vetter I, Borasio GD, Goody RS, et al. Kinetic and structural analysis of the Mg(2+)-binding site of the guanine nucleotide-binding protein p21H-ras. The Journal of biological chemistry. 1993;268(2):923-9.
48. Wong KA, Russo A, Wang X, Chen YJ, Lavie A, O'Bryan JP. A new dimension to Ras function: a novel role for nucleotide-free Ras in Class II phosphatidylinositol 3-kinase beta (PI3KC2beta) regulation. PLoS One. 2012;7(9):e45360.
49. Liu H, Li Q, Cheng X, Wang H, Wang G, Hao H. UDP-glucuronosyltransferase 1A determinates intracellular accumulation and anti-cancer effect of β-lapachone in human colon cancer cells. PLoS One. 2015;10(2):e0117051.
50. Li J, Byrne KT, Yan F, Yamazoe T, Chen Z, Baslan T, et al. Tumor Cell-Intrinsic Factors Underlie Heterogeneity of Immune Cell Infiltration and Response to Immunotherapy. Immunity. 2018;49(1):178-93 e7.
51. Kahan SM, Bakshi RK, Ingram JT, Hendrickson RC, Lefkowitz EJ, Crossman DK, et al. Intrinsic IL-2 production by effector CD8 T cells affects IL-2 signaling and promotes fate decisions, stemness, and protection. Sci Immunol. 2022;7(68):eabl6322.
52. Harrington LE, Janowski KM, Oliver JR, Zajac AJ, Weaver CT. Memory CD4 T cells emerge from effector T-cell progenitors. Nature. 2008;452(7185):356-60.
53. Khan I, Koide A, Zuberi M, Ketavarapu G, Denbaum E, Teng KW, et al. Identification of the nucleotide-free state as a therapeutic vulnerability for inhibition of selected oncogenic RAS mutants. Cell Rep. 2022;38(6):110322.
54. Coley AB, Ward A, Keeton AB, Chen X, Maxuitenko Y, Prakash A, et al. Pan-RAS inhibitors: Hitting multiple RAS isozymes with one stone. Adv Cancer Res. 2022;153:131-68.
55. Luchini C, Paolino G, Mattiolo P, Piredda ML, Cavaliere A, Gaule M, et al. KRAS wild-type pancreatic ductal adenocarcinoma: molecular pathology and therapeutic opportunities. J Exp Clin Cancer Res. 2020;39(1):227.

56. di Magliano MP, Logsdon CD. Roles for KRAS in pancreatic tumor development and progression. Gastroenterology. 2013;144(6):1220-9.
57. Genovese G, Carugo A, Tepper J, Robinson FS, Li L, Svelto M, et al. Synthetic vulnerabilities of mesenchymal subpopulations in pancreatic cancer. Nature. 2017;542(7641):362-6.
58. Sheffels E, Kortum RL. The Role of Wild-Type RAS in Oncogenic RAS Transformation. Genes (Basel). 2021;12(5).
59. Khan HY, Nagasaka M, Li Y, Aboukameel A, Uddin MH, Sexton R, et al. Inhibitor of the Nuclear Transport Protein XPO1 Enhances the Anticancer Efficacy of KRAS G12C Inhibitors in Preclinical Models of KRAS G12C-Mutant Cancers. Cancer Res Commun. 2022;2(5):342-52.
60. Molina-Arcas M, Moore C, Rana S, van Maldegem F, Mugarza E, Romero-Clavijo P, et al. Development of combination therapies to maximize the impact of KRAS-G12C inhibitors in lung cancer. Sci Transl Med. 2019;11(510).
61. Lee SH, Yun S, Lee J, Kim MJ, Piao ZH, Jeong M, et al. RasGRP1 is required for human NK cell function. J Immunol. 2009;183(12):7931-8.
62. Iborra S, Ramos M, Arana DM, Lazaro S, Aguilar F, Santos E, et al. N-ras couples antigen receptor signaling to Eomesodermin and to functional CD8+ T cell memory but not to effector differentiation. J Exp Med. 2013;210(7):1463-79.
63. Perez de Castro I, Diaz R, Malumbres M, Hernandez MI, Jagirdar J, Jimenez M, et al. Mice deficient for N-ras: impaired antiviral immune response and T-cell function. Cancer Res. 2003;63(7):1615-22.
64. Iborra S, Soto M, Stark-Aroeira L, Castellano E, Alarcon B, Alonso C, et al. H-ras and N-ras are dispensable for T-cell development and activation but critical for protective Th1 immunity. Blood. 2011;117(19):5102-11.
65. Kortum RL, Rouquette-Jazdanian AK, Samelson LE. Ras and extracellular signal-regulated kinase signaling in thymocytes and T cells. Trends Immunol. 2013;34(6):259-68.

Figure legends:

Figure 1. Potent and selective anticancer activity of ADT-007. (A) ADT-007 potently inhibits the growth of mutant (G13D) KRAS mutant HCT116 CRC cells while WT RAS, mutant BRAF (V600E) HT29 CRC cells have reduced sensitivity. Cell growth was measured by Cell Titer Glo assay following 72 hours of treatment. Activated RAS (GTP-RAS) levels from each cell line were pulled down from 200 µg of cell lysate using 60 µg of GST-RAF-RBD/glutathione agarose. Detection of active RAS was performed by WB the pull-down output with a pan-RAS antibody. Total RAS and GAPDH levels were determined by WB with the whole cell lysate. (B) ADT-007 potently and selectively inhibits colony formation of HCT116 cells without affecting HT29 cells following 10 days of treatment. Images on the right show complete inhibition of colony formation. Samples were run in triplicate. Counts are represented as colonies/well. Error bars represent standard deviation (SD). (C) ADT-007 induces apoptosis of HCT116 cells, but not HT29 cells as measured by Annexin V expression following 48 hours of treatment. Findings are representative of 3 independent experiments. Data is represented as a fold difference in annexin V, which was calculated with the following equation (% annexin V in ADT-007 treated/% annexin V in vehicle (DMSO) = fold induction of apoptosis. (D) ADT-007 induces G2/M cell cycle arrest in HCT116 but not HT29 cells following 24 hours of treatment. Experiments were performed in triplicate and error bars represent standard deviation (SD). (E) Growth inhibitory activity of ADT-007 vs vehicle (DMSO) in HCT116 cells is associated with increased expression of histone 3B, a marker of mitotic arrest.

Figure 2. Potent and selective anticancer activity of ADT-007 in PDAC cell lines. (A) Active RAS levels in a panel of PDAC cell lines as measured by RAS-RBD pulldown assays described in Figure 1. (B) ADT-007 inhibition of colony formation by pancreatic tumor cell lines. The assay was terminated for each respective cell line when colonies in its vehicle control group reached a size of approximately 50 cells. Differences in colony counts of MIA PaCa-2, CFPAC-1, PANC-1,

and SW-1990 at 12 nM were statistically significant from vehicle controls, while BxPC-3 exhibited no statistically significant reduction in colony count. Curves are graphed as the mean of three replicates ± SEM. (One-way ANOVA; *p<0.05 vs. the vehicle (DMSO) control for each indicated cell line). Results shown are representative of at least two independent experiments.(C) ADT-007 potently induces G2/M arrest in mutant KRAS MIA-PaCa-2 PDAC cells compared with WT RAS BxPC-3 PDAC cells following 24 hours of treatment. (D) Time-dependent induction of apoptosis in MIA-PaCa-2 cells by ADT-007 as measured by caspase cleavage. (E) Growth inhibitory activity of ADT-007 in monolayer or spheroid cultures of MIA-PaCa-2 cells as measured by Cell Titer Glo assay.

Figure 3. Comparison of the anticancer activity of ADT-007 with mutant specific KRAS inhibitors. (A) Growth inhibitory activity of ADT-007 and AMG-510 in mutant G12C mutant MIA-PaCa-2 PDAC cells following 72 hours of treatment as measured by Cell Titer Glo assay. Samples were run in triplicate and error bars represent standard deviation (SD). (B) Inhibition of colony formation by ADT-007 and AMG-510 in G12C mutant MIA-PaCa-2 PDAC cells following 10 days of treatment. Data is representative of 3 independent experiments. (C) Growth inhibitory activity of ADT-007 and G12C KRAS mutant inhibitors, AMG-510 and MRTX 1257-resistant MIA-PaCa-2 cells after 72 hours of treatment (*p <0.05 from parental MIA-PaCa-2 cells).Samples were run in triplicate and error bars represent standard deviation (SD). Data is representative of 2 independent experiments. (D) Murine Lewis Lung cancer cells harboring both KRAS-G12C and NRAS-Q61H mutations were sensitive to ADT-007 but not to AMG-510.

Figure 4. RAS-selective growth inhibition of ADT-007 in isogenic colon cancer cell pairs. (A) HRAS-G12V transfection of KRAS WT HT29 cells induces sensitivity to ADT-007. (B) RAS-PRB pull-down assays confirming transfection of RAS WT cells with activated RAS G12V mutant (GTP-RAS-green star) while parental and retroviral control (retro) cells with WT *RAS* have reduced sensitivity. (B) RAS activation (*****) in HRAS HT29 cells was confirmed by RBD pull-

down (*RAS-PD*) followed by WB using total RAS antibody. Protein levels of total RAS and GAPDH were determined by WB in whole cell lysates**.**

Figure 5. Cellular thermal shift assay (CETSA) shows ADT-007 binds KRAS with high affinity in HCT116 but not HCT29 CRC cells. Non-denaturing lysates were incubated 4h with ADT-007 or DMSO, followed by 15 min heat shock at the 75% aggregation temperature. After removal of insoluble protein by centrifugation, remaining (stabilized) protein was detected by WB. Graphs show levels of compound stabilized KRAS compared with vehicle control. None-heat shocked KRAS was used as a loading control. The cyclic guanosine monophosphate phosphodiesterase 10 isozyme (PDE10) was used as a negative control.

Figure 6. ADT-007 reduces activated RAS levels and inhibits RAS signaling in mutant KRAS HCT116 CRC cells. Cells were treated for 18 hours and lysates probed for activated RAS by RAS-RBD pulldown assays or for inhibition of RAS signaling using phospho-specific antibodies by WB analysis. Data is representative of 3 independent experiments.

Figure 7. Inhibition of activated RAS (RAS-GTP) in MIA PaCa-2 PDAC cells by ADT-007. (A) ADT-007 reduces RAS-GTP levels in cells grown under basal cell culture growth conditions. Cells were treated with vehicle or ADT-007 for 24 hours in complete growth media (with 10% FBS). (B) ADT-007 reduces RAS-GTP levels in cells under serum-starved conditions. Cells were treated with vehicle or ADT-007 for 24 hours in serum-free media. (C) ADT-007 reduces RAS-GTP levels under EGF-stimulated conditions. Cells were treated with vehicle or ADT-007 for 24 hours in serum-free media and subsequently stimulated with 30 ng/mL EGF for 10 minutes. Activated RAS levels were measured by RAS-RBD pull-down and detection by WB as described in Figure 1.

Figure 8. ADT-007 inhibits activated RAS among all three RAS isoforms in MIA PaCa-2 PDAC cells. Cells were treated with vehicle (DMSO) or ADT-007 for 24 hours in serum-free

media and subsequently stimulated with 30 ng/mL EGF for 10 minutes. The active RAS pull-down was performed as described in Figure 1. WB was performed with a pan RAS antibody, along with isoform-specific RAS antibodies. Results shown are representative of 3 independent experiments demonstrating effects observed on RAS isoforms.

Figure 9. Inhibition of MAPK and PI3K/AKT signaling by ADT-007 in MIA PaCa-2 PDAC cells. The MEK inhibitor U0126 (2 µM), and the PI3K inhibitor LY294002 (10 µM) were used as positive controls for inhibition of both pathways, inhibition of MAPK activation, and inhibition of AKT activation, respectively. Cells were treated with vehicle (DMSO) or compounds for 24 hours in serum-free media and subsequently stimulated with 30 ng/mL EGF for 10 minutes. Detection of phospho-protein levels was performed by WB. Results shown are representative of at least three independent experiments.

Figure 10. **Molecular modeling of ADT-007 binding to WT KRAS.** GDP-bound KRAS (Pdb code 4OBE) with Mg+2 shown in gray. ADT-007 fits into a groove that partially overlaps the nucleotide binding domain. The docking score of GDP (physiological substrate of RAS) was comparable to ADT-007 (-11.4 vs -11.1) and was reduced to -7.6 by ADT-007 binding.

Figure 11. ADT-007 selectively inhibits GTP binding to Nucleotide-Free recombinant KRAS WT protein. (A) ADT-007 inhibits MANT-GTP binding to recombinant KRAS under nucleotide-free treatment conditions. Vehicle (DMSO) or ADT-007 (5 µM) were incubated with nucleotide-free RAS prior to the addition of MANT-GTP. NF-KRAS was generated by incubating 1 µM GDP-bound KRAS with 20 mM EDTA to stimulate nucleotide exchange in the presence of DMSO (blue) or ADT-007 (green) for 1 hr. The reaction was started by adding 750 nM MANT-GTP to load KRAS with GTP. Binding kinetics with no nucleotide exchange (no EDTA plus DMSO) is shown in black. The curves represent the mean of three replicates. B) ADT-007 (5 µM) showed only modest activity when added at the same time as MANT-GTP. Curves show

the kinetics of MANT-GTP binding to RAS in the presence of vehicle (DMSO) or ADT-007 and represent the mean of three replicates.

Figure 12. ADT-007 inhibits GTP loading to block RAS-effector binding using recombinant WT KRAS. (A) ADT-007 inhibited GTP loading when added before GTP addition. (B) ADT-007 did not inhibit RAS effector binding when added after GTP loading, but before the active RAS pull-down. Recombinant WT KRAS was incubated 1 hr with EDTA (A) or vehicle (B) prior to treatment with ADT-007 (1 hr) followed by GTPγS (100 μM). RAS effector binding was measured using recombinant WT KRAS with a RAS GTP loading/GST-RAF-RBD pulldown assay as described in Figure 1. Note GTP stimulation of RAS-RAF binding under both conditions.

Figure 13. ADT-007 effect on HSQC NMR spectra of Nucleotide-Free KRAS (1-166). Recombinant WT KRAS was dialyzed following EDTA treatment to remove Mg and bound nucleotide. NF KRAS was then treated with either DMSO (blue) or ADT-007 (red) followed by NMR spectroscopy. ADT-007 induced pronounced signal attenuation in the P-loop (left) as well as chemical shifts or signal attenuation of several other residues throughout the protein.

Figure 14. Pharmacokinetics and Metabolism of ADT-007. (A) Plasma ADT-007 concentration after single oral (100 mg/kg); SC or IP (10 mg/kg) administration.

(B-C). Intracellular concentration and metabolism of ADT-007 *in vitro*. After 24 h treatment in vitro with 100 nM ADT-007, cells were collected. B) The ratio of glucuronidated ADT-007 to the unconjugated form was determined by peak-area comparison of the respective molecular mass by LC-MS/MS. * = below limit of detection. (C) Intracellular ADT-007 concentration was compared with a standard curve by LC-MS/MS following organic extraction. (D-E). The ratio of glucuronidated ADT-007 to the unconjugated form (D) and metabolic stability of ADT-007(E) in mouse liver microsome assay (LC-MC/MC).

Figure 15. ADT-007 inhibition of tumor growth and RAS signaling *in vivo*. (A) Growth inhibition of subcutaneous CT26 colon tumors in BALB/c mice by IT administration of ADT-007 (10 mg/kg, QD, days 10-23 after tumor implantation) (** $p<0.001$, **** $p<0.0001$, mean ± SE, n=12). (B) ADT-007 reduces activated RAS levels (RAS-RAF pull-down assay) and MAPK signaling (reduced p-C-RAF, p-MEK, and p-ERK) in excised tumors from mice shown in A after the last ADT-007 injection. Tumors were collected and cell lysates generated to evaluate activated RAS (RAS-RAF pulldown), phosphorylated RAF, MEK, and ERK levels by WB analysis. Each lane corresponds to a single mouse from the control or treatment (n=4) groups. GAPDH was used as a loading control.

Figure 16. ADT-007 inhibits subcutaneous tumor growth of KRAS mutated CRC and PDAC cell lines. ADT-007-mediated tumor growth inhibition of subcutaneous (A) G12V mutated PDX PDAC in NSG mice, (B) G12C mutated PDX PA2 PDAC in NSG mice, (C) G13D mutated human HCT116 CRC in athymic nude mice, or (D-F) mouse PDAC in C57BL/6 mice [(D) 2838c3, (E) 7160c2, and (F) 5363]. When tumors reached an average volume of 150 mm^3, tumor-bearing mice began receiving subcutaneous peri-tumoral (SQ) injections (5 mg/kg BID) or intratumoral (IT) injections (10 mg/kg QD) of ADT-007 or sham for a period of 14-21 days. Tumor growth was monitored by caliper measurements and calculation of tumor volumes. Statistical significance was calculated using one way ANOVA with is represented by * $p < 0.05$, ** $p < 0.01$, *** $p < 0.001$, **** $p < 0.0001$. Data is summarized as mean values and error bars indicating SEM.

Figure 17. ADT-007 increases gMDSC and mMDSC infiltrates into the 7160c2 PDAC TME. (A-D) At 21 days post treatment the proportions of tumor and myeloid cells were evaluated by multiparameter flow cytometry in the 7160c2 model. (A) The percentages of YFP^+ tumor cells were decreased in ADT-007 treated mice (n = 8) compared to Sham (n = 7). Data is the representative of two independent experiments in 7160c2 model. (B) The percentages of

CD11b$^+$ myeloid, CD11b$^+$ Ly6G$^+$ Ly6C$^+$ gMDSC, and CD11b$^+$ Ly6G$^-$ Ly6C^{hi} mMDSC were evaluated in ADT-007 treated (n = 21) and sham (n = 15) treated mice. Data is the aggregate of 2-3 independent experiments in the 7160c2 model. (**C**) The percentages of CD11b$^-$ CD11c^{hi} MHCII^{hi} XCR1$^+$ cDC1 and CD11b$^+$ CD11c^{hi} MHCII^{hi} CD172α$^+$ cDC2 subsets did not change in ADT-007 (n = 21) and Sham (n = 15) treated mice. Data is representative of aggregates of 2-3 experiments in 7160c2 model. (D) The percentages of CD11b$^+$ Ly6G$^-$ Ly6C$^-$ F4/80$^+$ macrophage and median fluorescent expression of MHCII and CD206 were evaluated in ADT-007 (n = 7- 21) and sham (n = 7- 15) treated mice. The percentages of macrophage are an aggregate of 2-3 independent experiments and MFI of MHCII and CD206 is representative of two independent experiments. (E-H) At 17 days post treatment the proportions of tumor and myeloid cells were evaluated by multiparameter flow cytometry in the 2838c3 subcutaneous model. (E) The percentages of YFP$^+$ tumor cells were decreased in ADT-007 treated mice (n = 8) compared to Sham (n = 8). Data representative of two independent experiments in 2838c3 model. (F) The percentages of CD11b$^+$ myeloid, CD11b$^+$ Ly6G$^+$ Ly6C$^+$ gMDSC, and CD11b$^+$ Ly6G$^-$ Ly6C^{hi} mMDSC were evaluated in ADT-007 treated (n = 11) and sham (n = 11) treated mice. Data is the aggregate of two independent experiments in the 2838c3 model. (G) The percentages of CD11b$^-$ CD11c^{hi} MHCII^{hi} XCR1$^+$ cDC1 and CD11b$^+$ CD11c^{hi} MHCII^{hi} CD172α$^+$ cDC2 subsets did not change in ADT-007 (n = 11) and Sham (n = 11) treated mice. Data is representative of aggregates of two experiments in 2838c3 model. (H) The percentages of CD11b$^+$ Ly6G$^-$ Ly6C$^-$ F4/80$^+$ macrophage and median fluorescent expression of MHCII and CD206 were evaluated in ADT-007 (n = 8-11) and sham (n = 8-11) treated mice. The percentages of macrophage are an aggregate of two independent experiments and MFI of MHCII and CD206 is representative of two independent experiments. For all statistical comparisons, p-values were determined by Student's unpaired t-test. Data is summarized as mean values and error bars indicate SD.

Figure 18. ADT-007 induces T cell activation and enhances cytotoxic function in PDAC mouse models. Tumor Growth inhibition of (**A**) 2838c3 and (**B**) 7160c2 PDAC tumor bearing C57BL/6 WT vs. C57BL/6 Rag $1^{-/-}$ mice. At 21 days post treatment (**C-D**) proportions of (**C**) $CD4^+$ $Foxp3^-$, $CD4^+$ $Foxp3^+$, $CD8^+$ T cells, (**D**) NK T, γδ T, and NK cells were determined by multi-parameter flow cytometry (**Figure S8**) in ADT-007 (n = 14) and sham (n = 14) treated mice. Data is aggregated from two independent experiments. (**E**) Expression of CD44 and CD62L in $CD3^+$ $CD4^+$ $Foxp3^+$ (Treg), $CD3^+$ $CD4^+$ $Foxp3^-$, $CD3^+$ $CD8^+$ (CTL), and $CD3^+$ $TCR\gamma\delta^+$ (γδ T) were evaluated by multi-parameter flow cytometry to determine percentages of naïve ($CD44^-$ $CD62L^+$), pre-effector ($CD44^-$ $CD62L^-$), effector memory ($CD44^+$ $CD62L^-$), and central memory T cells ($CD44^+$ $CD62L^+$) in ADT-007 (n = 14) and sham (n = 14) treated mice. (**F-H**) Cytokine (IL-2, granzyme B, IFNγ, and TNFα) production from (**F**) $CD4^+$, (**G**) $CD8^+$, and (**H**) γδ T cells were evaluated after 5-hour stimulation with PMA/ionomycin in the presence of brefeldin A in ADT-007 (n = 8) or sham (n = 8) treated mice. Data is representative of two independent experiments. For all statistical comparisons, p-values were determined by Student's unpaired t-test. Data is summarized as mean values and error bars indicating SD.

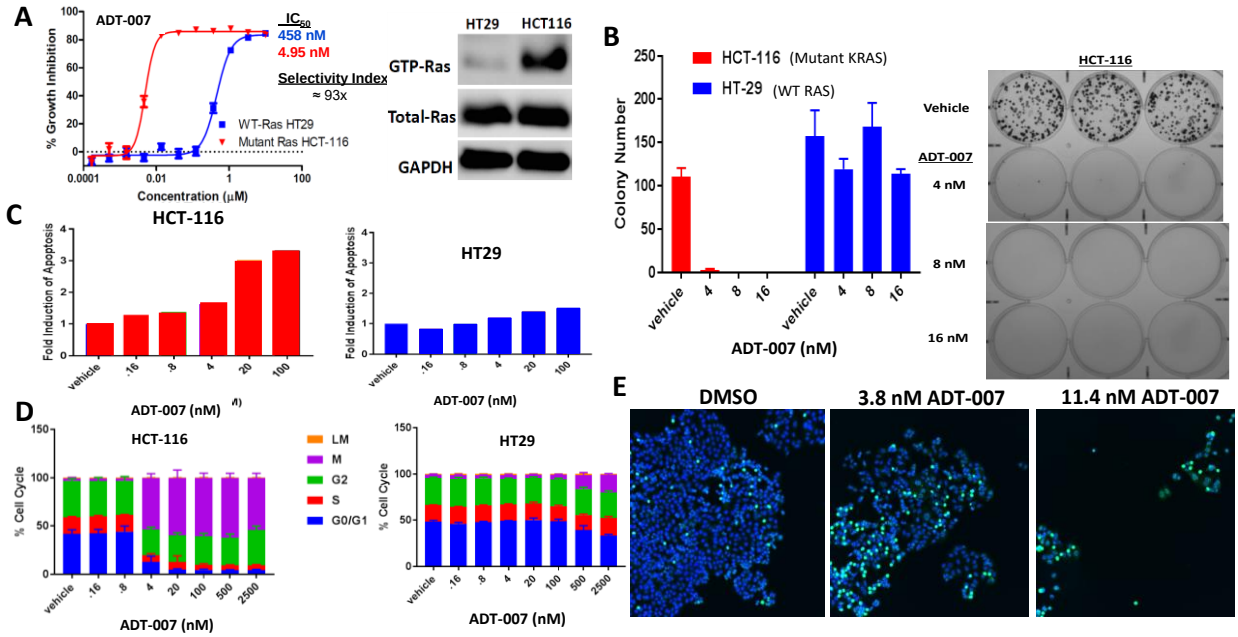
A
ADT-007
% Growth Inhibition
Concentration (μM)
IC50
458 nM
4.95 nM
Selectivity Index
≈ 93x
WT-Ras HT29
Mutant Ras HCT-116
HT29
HCT116
GTP-Ras
Total-Ras
GAPDH
B
HCT-116 (Mutant KRAS)
HT-29 (WT RAS)
Colony Number
ADT-007 (nM)
Vehicle
ADT-007
4 nM
8 nM
16 nM
HCT-116
C
HCT-116
HT29
Fold Induction of Apoptosis
ADT-007 (nM)
D
HCT-116
HT29
% Cell Cycle
LM
M
G2
S
G0/G1
ADT-007 (nM)
E
DMSO
3.8 nM ADT-007
11.4 nM ADT-007

Figure 1

Mutation Status	IC_{50}, Cell-based Assay (nM)	Cell Line	Tumor Origin	Genotype
KRAS G12C	2.1	Mia PaCa-2	Pancreatic	Mutant RAS
KRAS G12D	2.4	PANC-1	Pancreatic	
KRAS G12D	6.3	SW-1990	Pancreatic	
KRAS G12S	6.8	A549	Lung	
KRAS G12V	5.8	CFPAC-1	Pancreatic	
KRAS G12V	6.5	SW480	Colon	
KRAS G13D	3.6	MDA-MB-231	Breast	
KRAS G13D	4.7	HCT116	Colon	
KRAS P121H	5.8	OVCAR8	Ovarian	
HRAS G12D	3.9	Hs578	Breast	
NRAS Q61K	2.1	SK-MEL-2	Melanoma	
NRAS Q61K	2.4	H1299	Lung	
WT RAS	19100	NHAEC	Normal Lung	WT RAS
WT RAS	9600	H322	Lung	
WT RAS	>50000	NCM-460	Normal Colon	
WT RAS	>25000	SK-MEL-28	Melanoma	
WT RAS/mut. BRAF	350	OV90	Ovarian	WT RAS pathway activated downstream
WT RAS/mut. BRAF	512	HT29	Colon	
WT RAS /mut. BRAF	2500	BXPC3	Pancreatic	
WT RAS /mut. EGFR	3.9	H1975	Lung	RAS pathway activated upstream
WT RAS /mut. PDGFR	5.8	B16	Melanoma	
WT RAS/mut. NF1	1.6	U87MG	Glioblastoma	
WT RAS /mut. NF1	6.7	SKOV3	Ovarian	

Table 1. Sensitivity of tumor cells to ADT-007 is associated with high activated RAS levels. Growth IC_{50} values were determined by Cell Titer Glo assay following 72 hours of treatment.

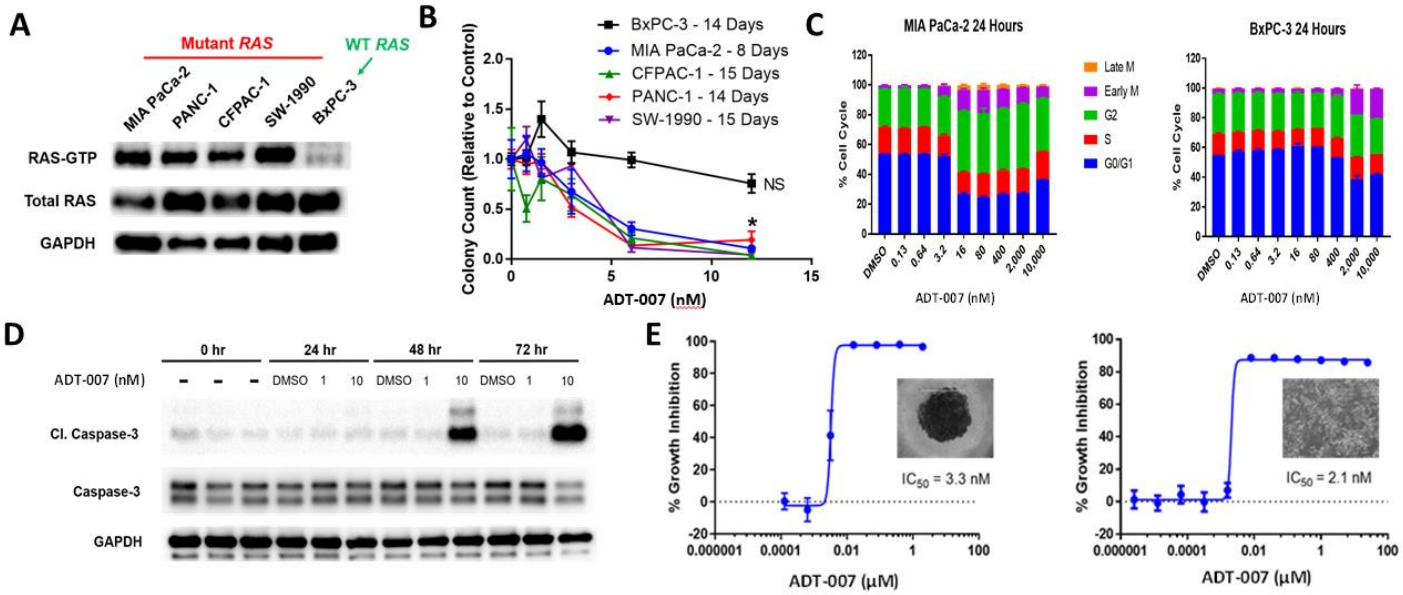
A
Mutant RAS
WT RAS
MIA PaCa-2
PANC-1
CFPAC-1
SW-1990
BxPC-3
RAS-GTP
Total RAS
GAPDH
B
BxPC-3 - 14 Days
MIA PaCa-2 - 8 Days
CFPAC-1 - 15 Days
PANC-1 - 14 Days
SW-1990 - 15 Days
Colony Count (Relative to Control)
ADT-007 (nM)
NS
*
C
MIA PaCa-2 24 Hours
BxPC-3 24 Hours
% Cell Cycle
Late M
Early M
G2
S
G0/G1
ADT-007 (nM)
D
0 hr
24 hr
48 hr
72 hr
ADT-007 (nM)
DMSO
1
10
Cl. Caspase-3
Caspase-3
GAPDH
E
% Growth Inhibition
IC50 = 3.3 nM
IC50 = 2.1 nM
ADT-007 (μM)

Figure 2

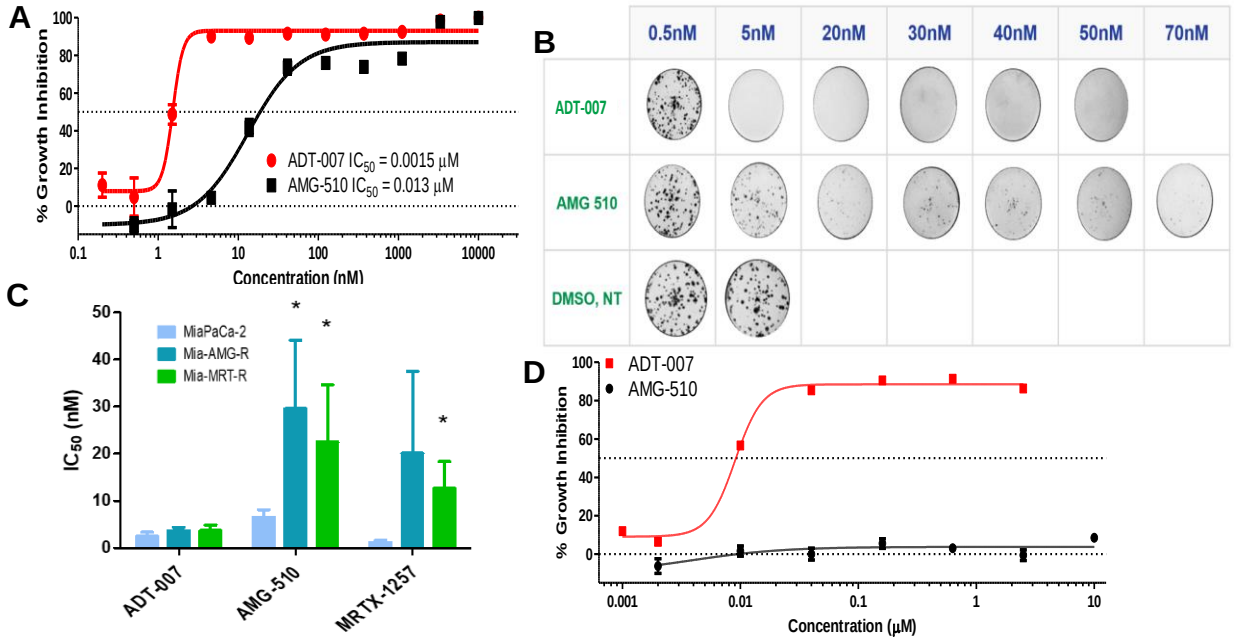
A
% Growth Inhibition
Concentration (nM)
ADT-007 IC50 = 0.0015 µM
AMG-510 IC50 = 0.013 µM
B
0.5nM
5nM
20nM
30nM
40nM
50nM
70nM
ADT-007
AMG 510
DMSO, NT
C
IC50 (nM)
MiaPaCa-2
Mia-AMG-R
Mia-MRT-R
ADT-007
AMG-510
MRTX-1257
D
ADT-007
AMG-510
% Growth Inhibition
Concentration (µM)

Figure 3

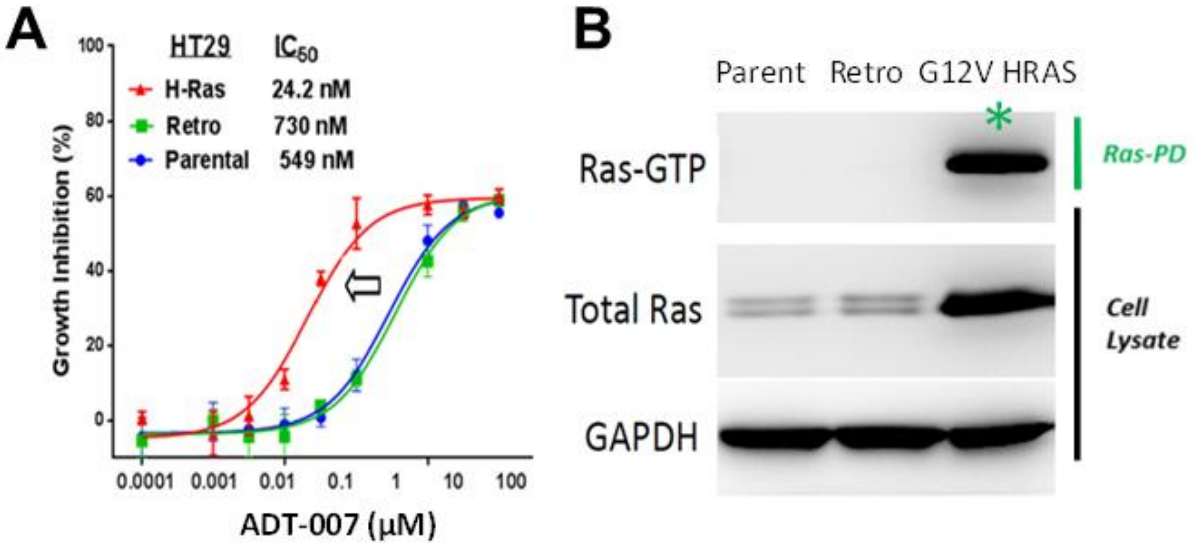
A
HT29
IC50
H-Ras
24.2 nM
Retro
730 nM
Parental
549 nM
Growth Inhibition (%)
100
80
60
40
20
0
0.0001
0.001
0.01
0.1
1
10
100
ADT-007 (μM)
B
Parent
Retro
G12V HRAS
Ras-GTP
Total Ras
GAPDH
Ras-PD
Cell Lysate

Figure 4

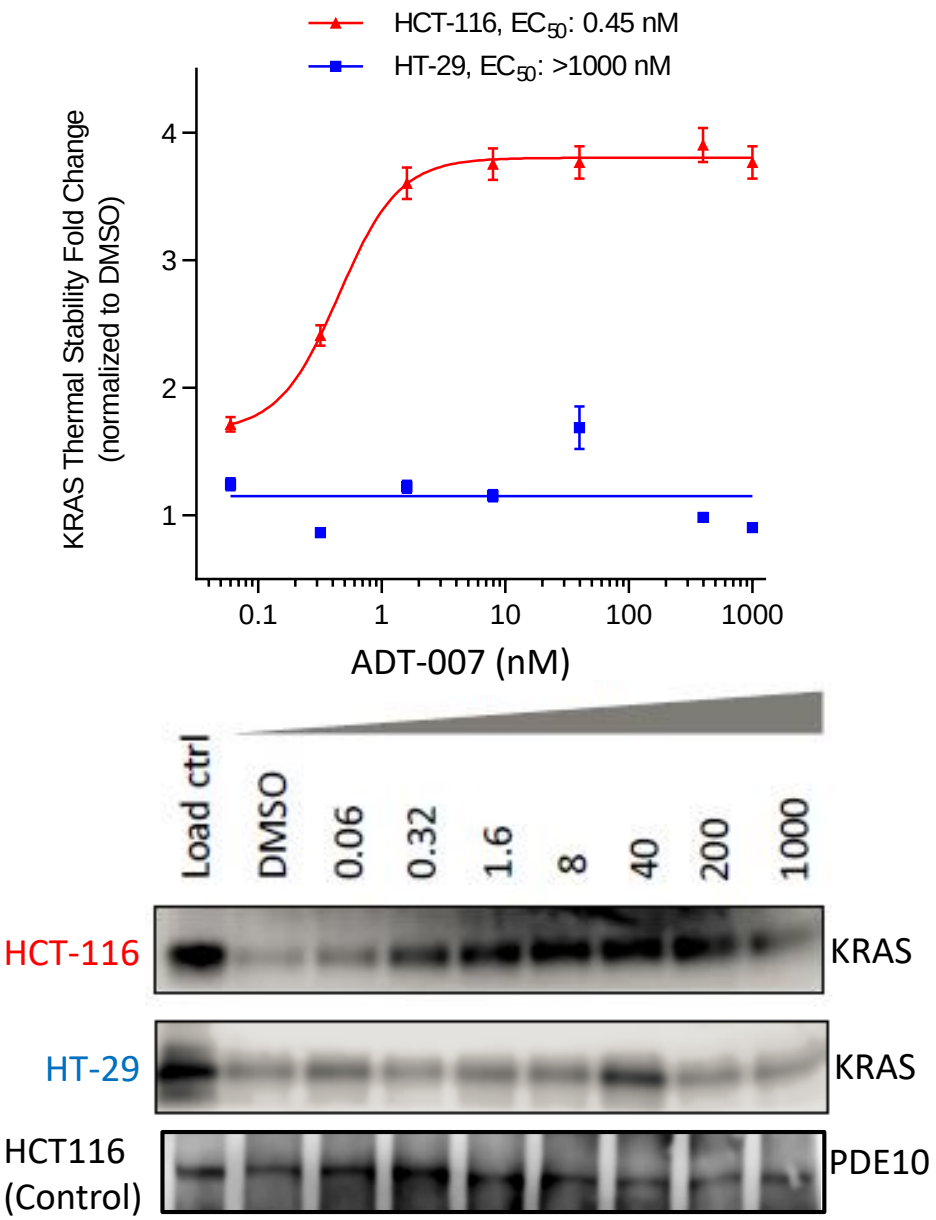
HCT-116, EC50: 0.45 nM
HT-29, EC50: >1000 nM
KRAS Thermal Stability Fold Change
(normalized to DMSO)
4
3
2
1
0.1
1
10
100
1000
ADT-007 (nM)
Load ctrl
DMSO
0.06
0.32
1.6
8
40
200
1000
HCT-116
KRAS
HT-29
KRAS
HCT116
(Control)
PDE10

Figure 5

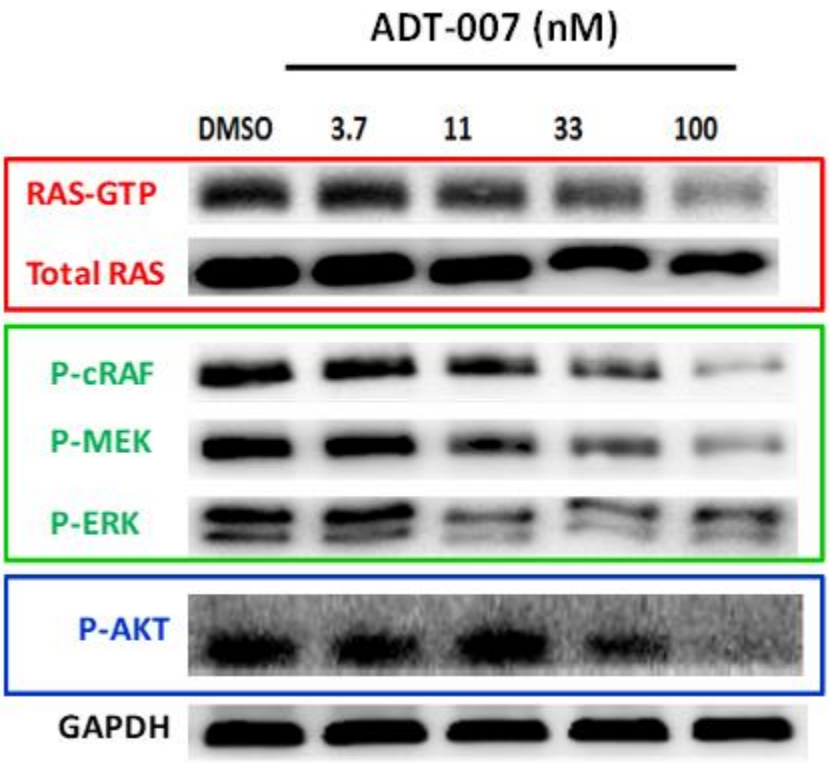
ADT-007 (nM)
DMSO
3.7
11
33
100
RAS-GTP
Total RAS
P-cRAF
P-MEK
P-ERK
P-AKT
GAPDH

Figure 6

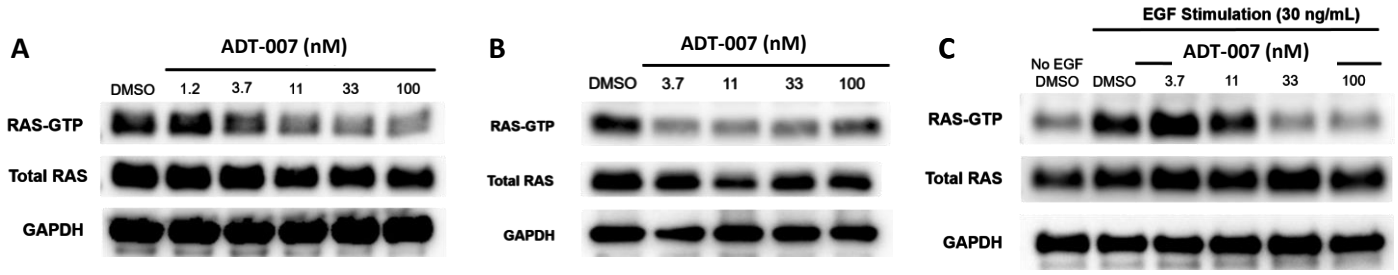
A
ADT-007 (nM)
DMSO
1.2
3.7
11
33
100
RAS-GTP
Total RAS
GAPDH
B
ADT-007 (nM)
DMSO
3.7
11
33
100
RAS-GTP
Total RAS
GAPDH
C
EGF Stimulation (30 ng/mL)
ADT-007 (nM)
No EGF
DMSO
DMSO
3.7
11
33
100
RAS-GTP
Total RAS
GAPDH

Figure 7

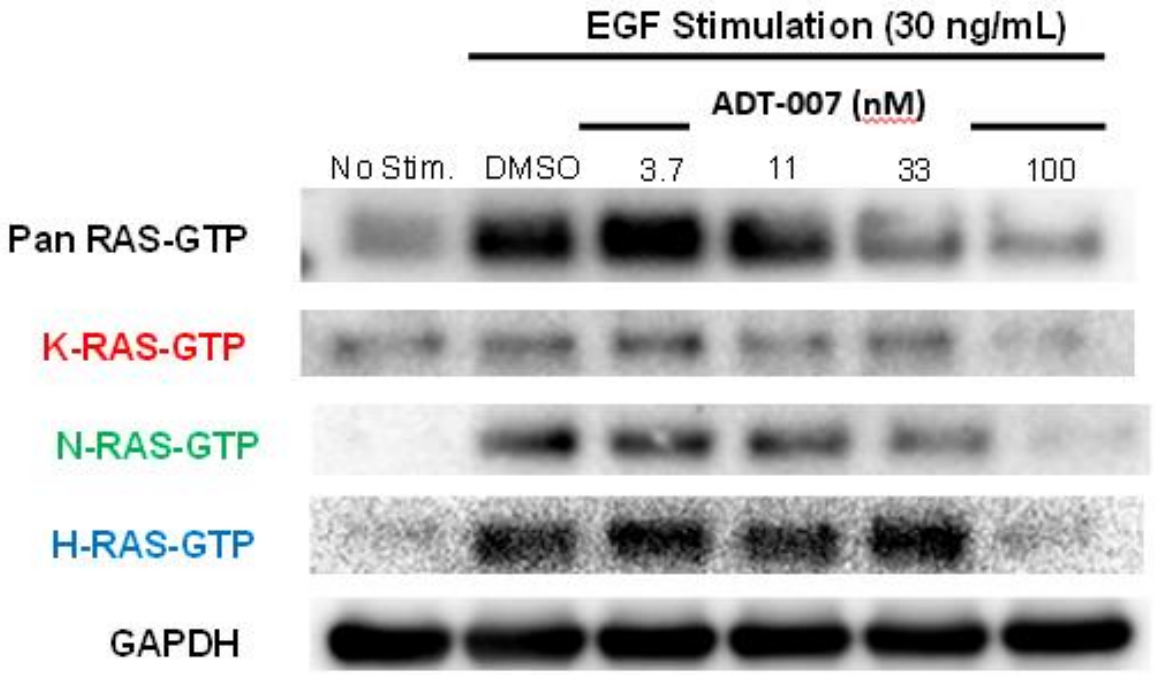
EGF Stimulation (30 ng/mL)
ADT-007 (nM)
No Stim.
DMSO
3.7
11
33
100
Pan RAS-GTP
K-RAS-GTP
N-RAS-GTP
H-RAS-GTP
GAPDH

Figure 8

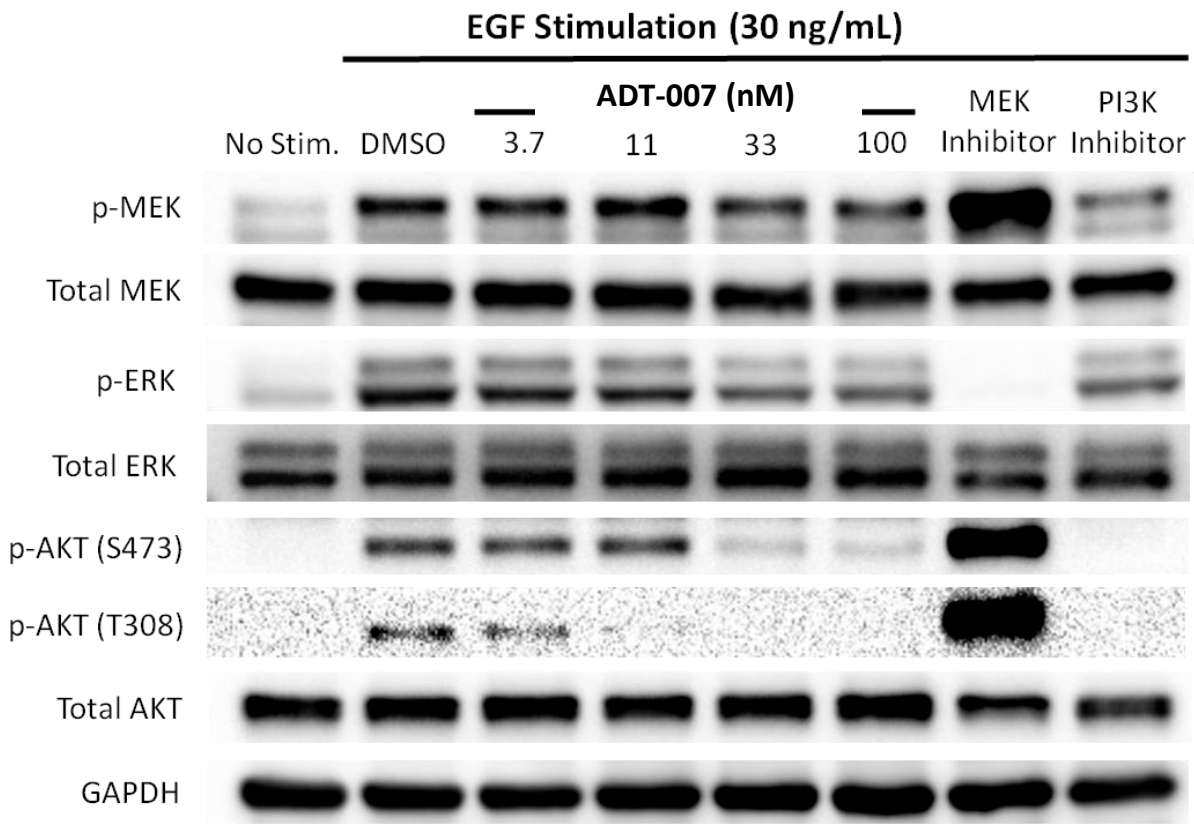
EGF Stimulation (30 ng/mL)
ADT-007 (nM)
No Stim.
DMSO
3.7
11
33
100
MEK Inhibitor
PI3K Inhibitor
p-MEK
Total MEK
p-ERK
Total ERK
p-AKT (S473)
p-AKT (T308)
Total AKT
GAPDH

Figure 9

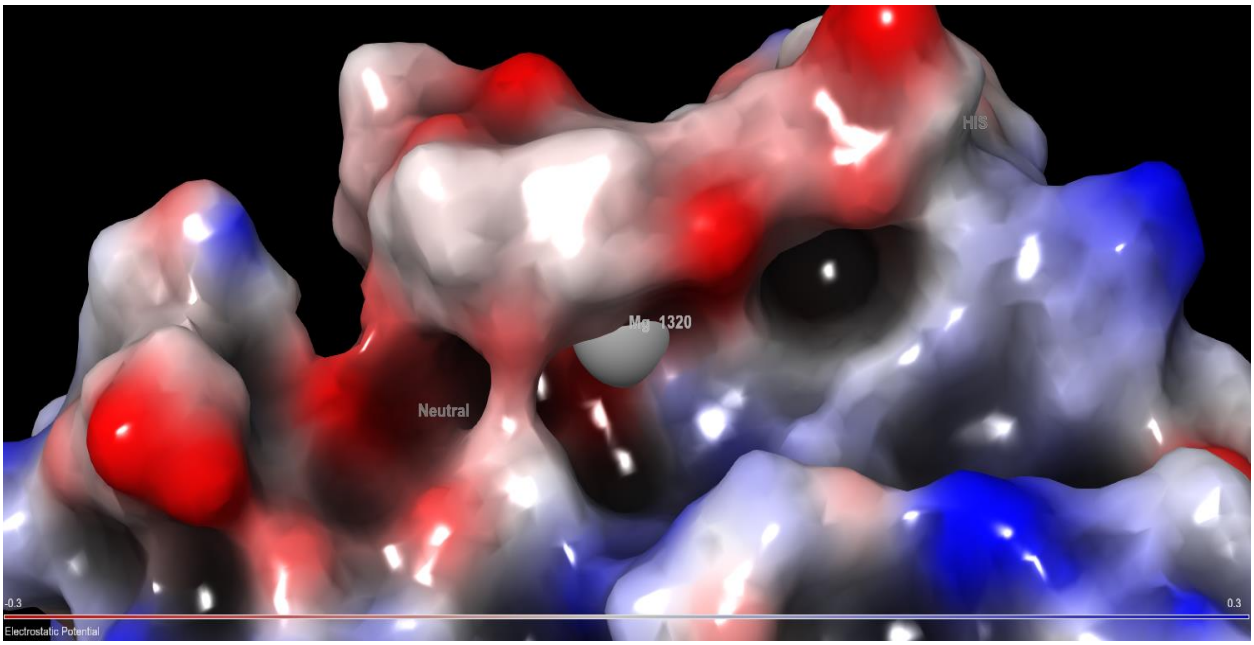

Figure 10

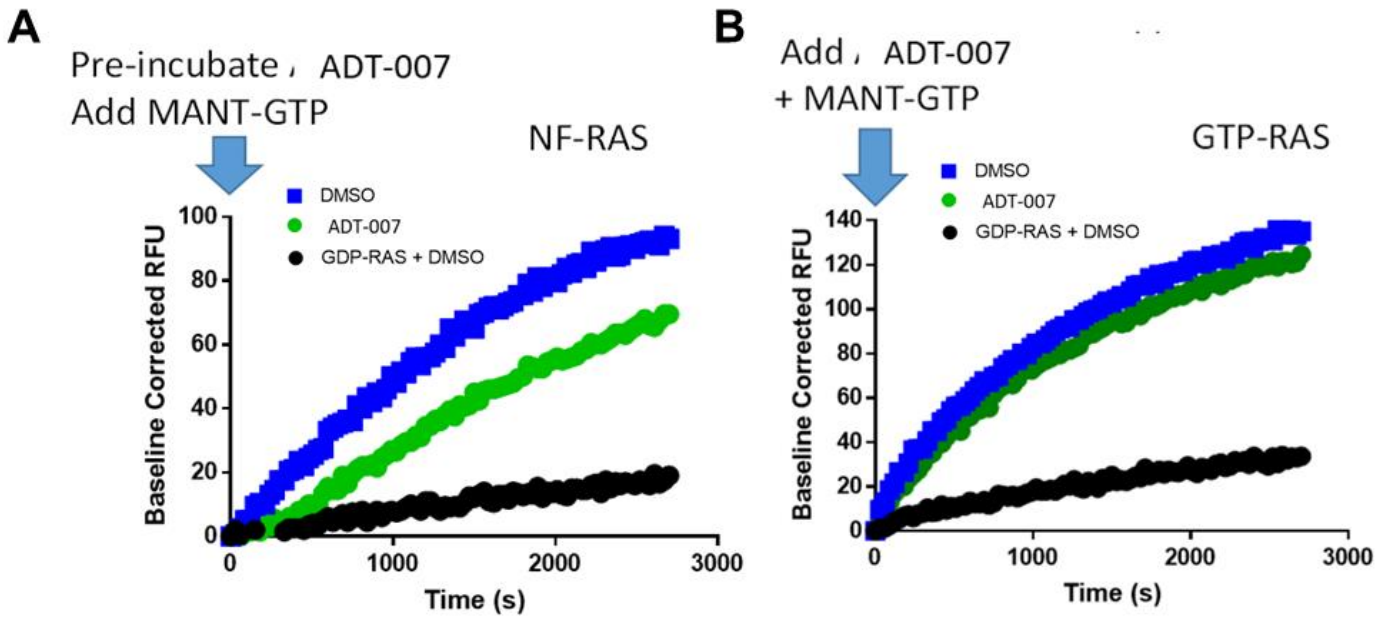
A
Pre-incubate， ADT-007
Add MANT-GTP
NF-RAS
DMSO
ADT-007
GDP-RAS + DMSO
Baseline Corrected RFU
Time (s)
B
Add， ADT-007
+ MANT-GTP
GTP-RAS
DMSO
ADT-007
GDP-RAS + DMSO
Baseline Corrected RFU
Time (s)

Figure 11

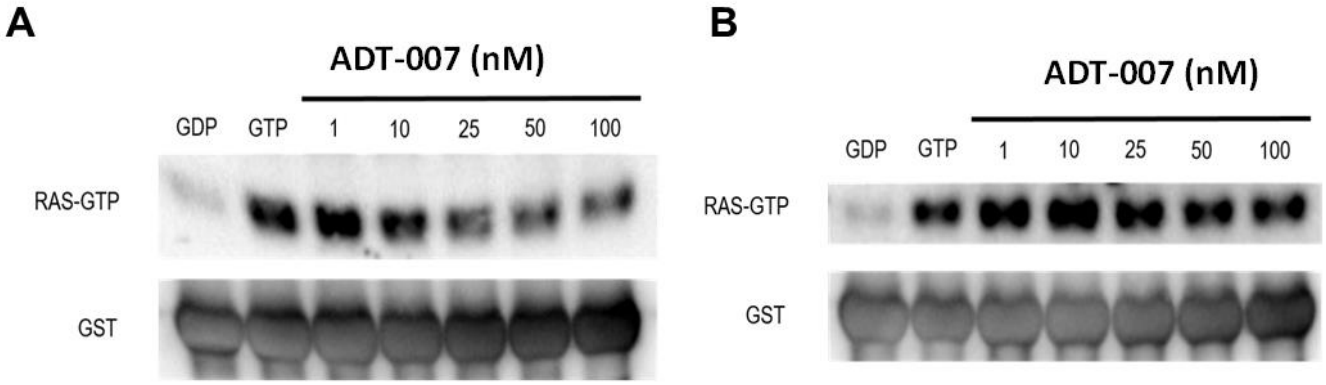
A
ADT-007 (nM)
GDP
GTP
1
10
25
50
100
RAS-GTP
GST
B
ADT-007 (nM)
GDP
GTP
1
10
25
50
100
RAS-GTP
GST

Figure 12

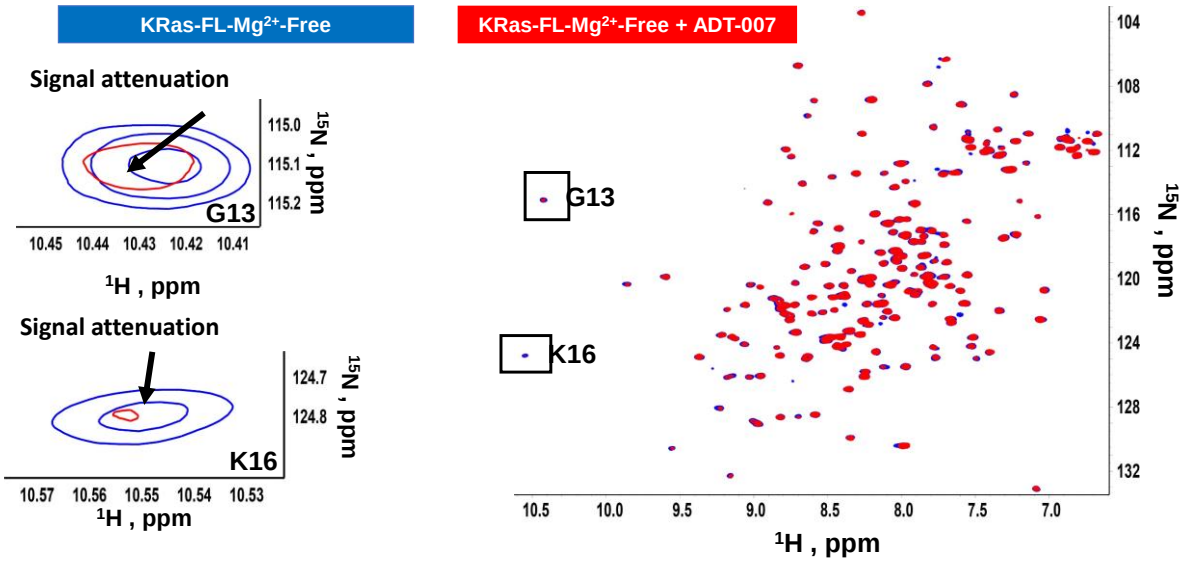
KRas-FL-Mg2+-Free
Signal attenuation
115.0
115.1
115.2
15N , ppm
G13
10.45 10.44 10.43 10.42 10.41
1H , ppm
Signal attenuation
124.7
124.8
15N , ppm
K16
10.57 10.56 10.55 10.54 10.53
1H , ppm
KRas-FL-Mg2+-Free + ADT-007
G13
K16
104
108
112
116
120
124
128
132
15N , ppm
10.5 10.0 9.5 9.0 8.5 8.0 7.5 7.0
1H , ppm

Figure 13

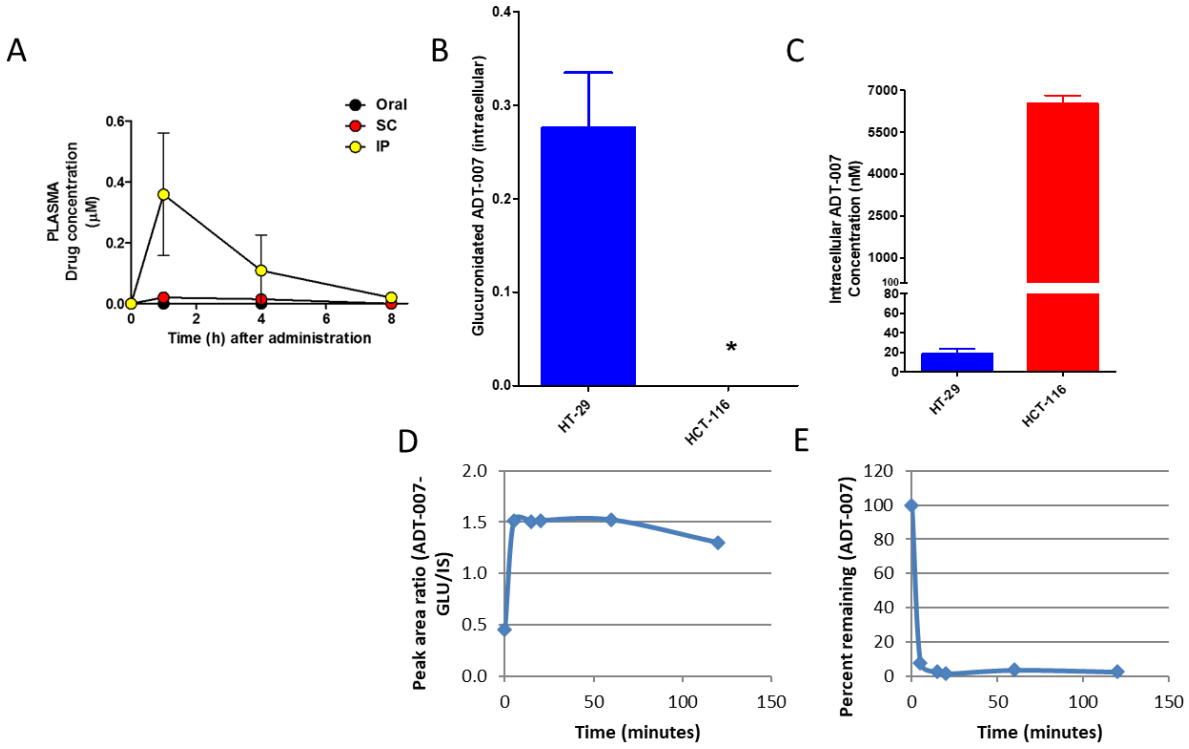
A
Oral
SC
IP
PLASMA Drug concentration (µM)
Time (h) after administration
B
Glucuronidated ADT-007 (intracellular)
HT-29
HCT-116
C
Intracellular ADT-007 Concentration (nM)
HT-29
HCT-116
D
Peak area ratio (ADT-007-GLU/IS)
Time (minutes)
E
Percent remaining (ADT-007)
Time (minutes)

Figure 14

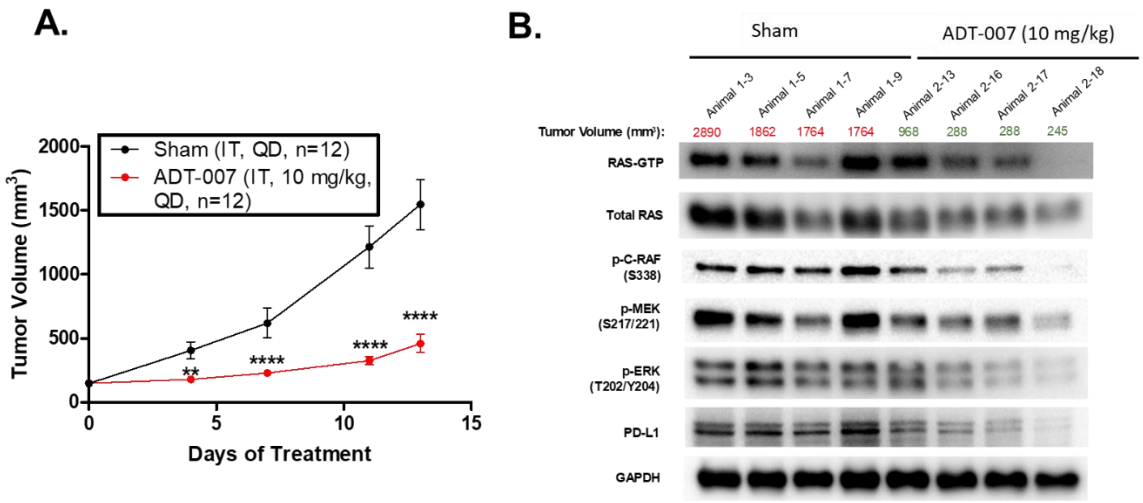
A.
Sham (IT, QD, n=12)
ADT-007 (IT, 10 mg/kg, QD, n=12)
Tumor Volume (mm3)
Days of Treatment
**
****
****
****
B.
Sham
ADT-007 (10 mg/kg)
Animal 1-3
Animal 1-5
Animal 1-7
Animal 1-9
Animal 2-13
Animal 2-16
Animal 2-17
Animal 2-18
Tumor Volume (mm3):
2890
1862
1764
1764
968
288
288
245
RAS-GTP
Total RAS
p-C-RAF (S338)
p-MEK (S217/221)
p-ERK (T202/Y204)
PD-L1
GAPDH

Figure 15

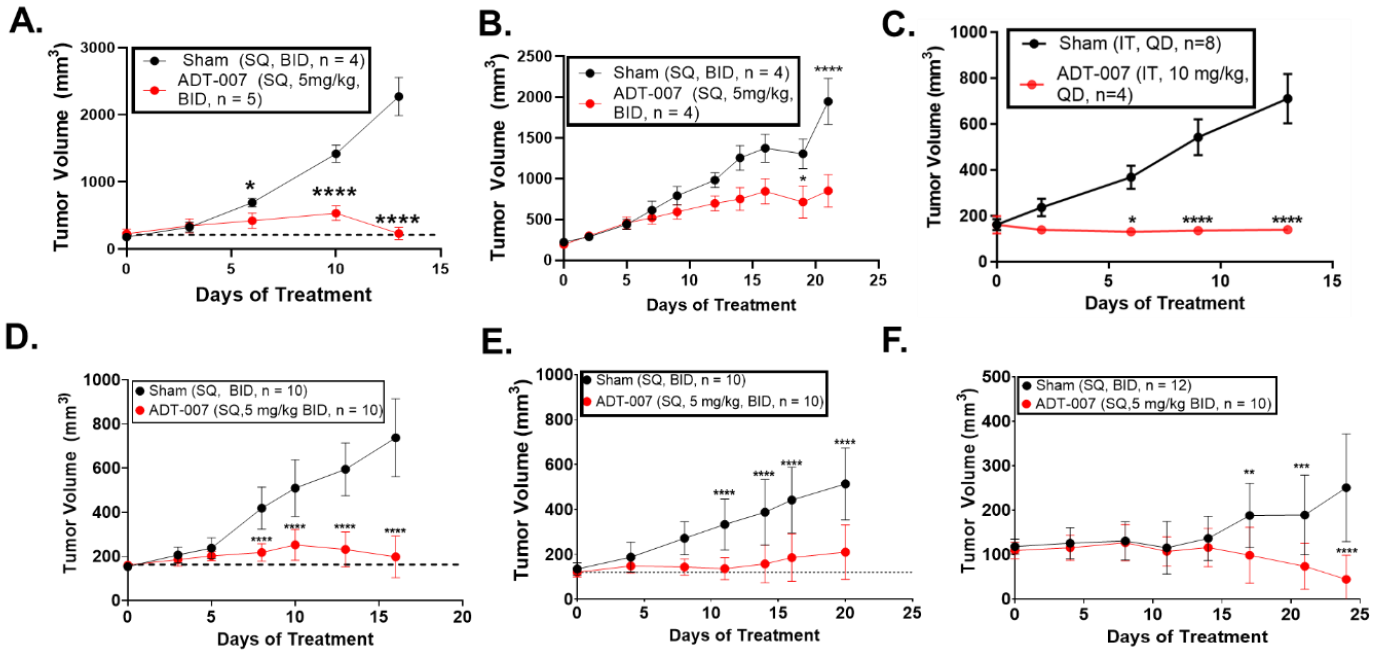
A.
Sham (SQ, BID, n = 4)
ADT-007 (SQ, 5mg/kg, BID, n = 5)
Tumor Volume (mm3)
Days of Treatment
B.
Sham (SQ, BID, n = 4)
ADT-007 (SQ, 5mg/kg, BID, n = 4)
Tumor Volume (mm3)
Days of Treatment
C.
Sham (IT, QD, n=8)
ADT-007 (IT, 10 mg/kg, QD, n=4)
Tumor Volume (mm3)
Days of Treatment
D.
Sham (SQ, BID, n = 10)
ADT-007 (SQ,5 mg/kg BID, n = 10)
Tumor Volume (mm3)
Days of Treatment
E.
Sham (SQ, BID, n = 10)
ADT-007 (SQ, 5 mg/kg, BID, n = 10)
Tumor Volume (mm3)
Days of Treatment
F.
Sham (SQ, BID, n = 12)
ADT-007 (SQ,5 mg/kg BID, n = 10)
Tumor Volume (mm3)
Days of Treatment

Figure 16

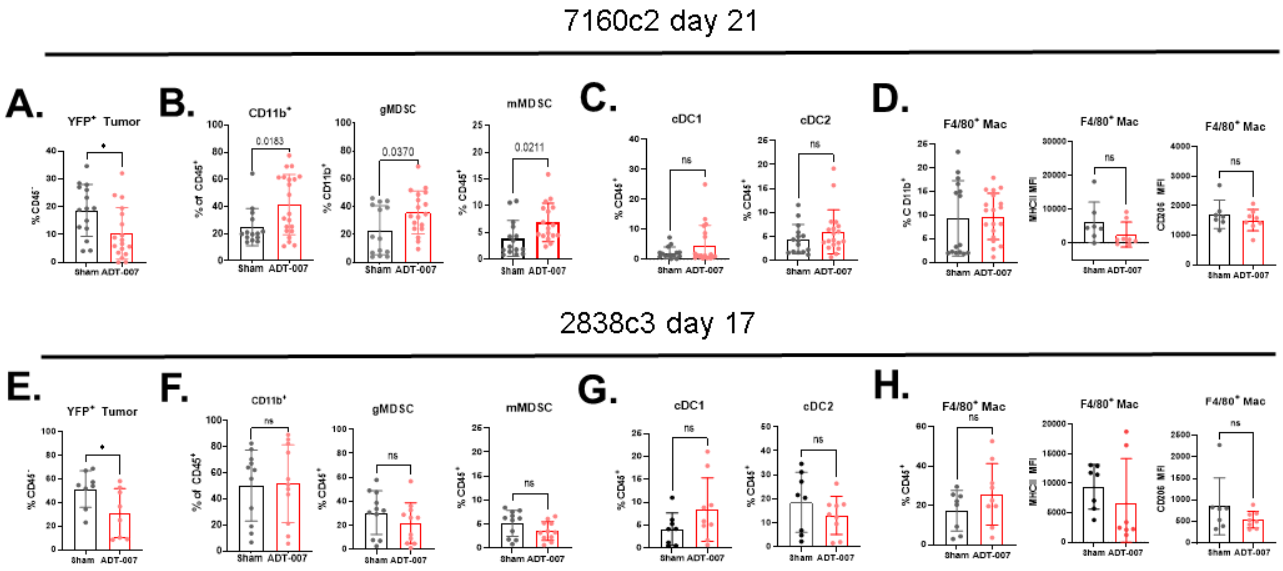
7160c2 day 21
A.
YFP+ Tumor
B.
CD11b+
gMDSC
mMDSC
0.0183
0.0370
0.0211
C.
cDC1
cDC2
D.
F4/80+ Mac
Sham
ADT-007
2838c3 day 17
E.
F.
G.
H.
ns

Figure 17

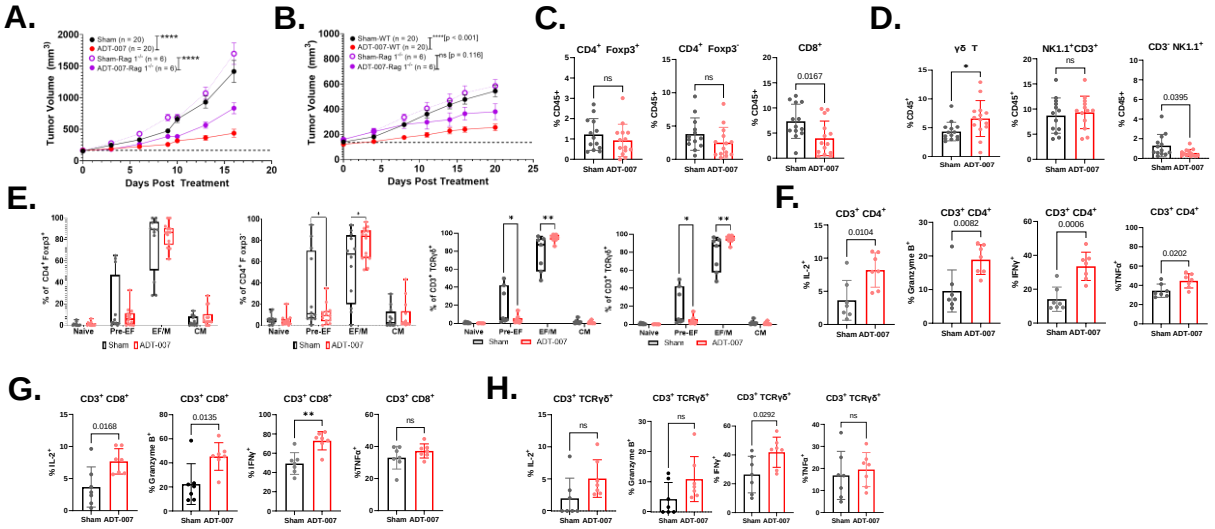
A.
B.
C.
D.
E.
F.
G.
H.
Tumor Volume (mm³)
Days Post Treatment
Sham (n = 20)
ADT-007 (n = 20)
Sham-Rag 1⁻/⁻ (n = 6)
ADT-007-Rag 1⁻/⁻ (n = 6)
Sham-WT (n = 20)
ADT-007-WT (n = 20)
****[p < 0.001]
ns [p = 0.116]
CD4⁺ Foxp3⁺
CD4⁺ Foxp3⁻
CD8⁺
γδ T
NK1.1⁺CD3⁺
CD3⁻ NK1.1⁺
% CD45⁺
Sham ADT-007
Naive
Pre-EF
EF/M
CM
% of CD4⁺ Foxp3⁺
% of CD4⁺ F oxp3⁻
% of CD3⁺ TCRγδ⁺
CD3⁺ CD4⁺
CD3⁺ CD8⁺
CD3⁺ TCRγδ⁺
% IL-2⁺
% Granzyme B⁺
% IFNγ⁺
%TNFα⁺
0.0167
0.0395
0.0104
0.0082
0.0006
0.0202
0.0168
0.0135
0.0292
ns

Figure 18